Growth of C_{60} on the Twofold Surface of Quasicrystal Al-Ni-Co

A thesis submitted in partial fulfilment of the requirements for the degree of Master of Physics

Charlotte Conway(201491680)

Supervised by Dr Hem Raj Sharma

April 2024

Declaration of Authorship

I, CHARLOTTE CONWAY, declare that the thesis entitled 'Growth of C60 on the Twofold Surface of Quasicrystal Al-Ni-Co' and the work presented in it are my own. I confirm that:

- This work was done wholly or mainly while in candidature for a research degree at this University.
- Where any part of this thesis has previously been submitted for a degree or any other qualification at this University or any other institution, this has been clearly stated.
- Where I have consulted the published work of others, this is always clearly attributed.
- Where I have quoted from the work of others, the source is always given. With the exception of such quotations, this thesis is entirely my own work.
- I have acknowledged all main sources of help. Where the thesis is based on work done by myself jointly with others, I have made clear exactly what was done by others and what I have contributed myself.

Abstract

This project aimed to investigate the twofold quasicrytaline surface of Al-Ni-Co through the growth of C_{60}, imaged using scanning tunnelling microscopy. It was hypothesised that the C_{60} molecules would adsorb preferentially to nickel atomic sites, forming a one dimensional Fibonacci chain. The surface was successfully prepared and imaged before being dosed with C_{60} molecules and imaged again.

From these images, the surface was determined to be quasicrystaline through the measurements of the step heights, with the short and long sections in line with expectations (5 Å and 8 Å respectively). The clean surface was characterised and the interatomic spacing in the periodic and aperiodic directions were found to be consistent with expectations for the surface (2 Å for periodic, 5 Å and 8 Å for quasiperiodic). Both surfaces (before and after dosing) were related to each other, showing the same long and short quasiperiodic spacing.

The deposition of C_{60} was successful and has been deemed to be non-arbitrary, suggesting preferential adsorption. From analysis of the images it was seen that there were two kinds of adsorption sites which depended on the position of the nickel and cobalt atoms. Both of these adsorption sites were observed to be LL sites, where the C_{60} molecules were adsorbing between two long sections on the atomic surface. The images of the surface were compared to a model of the structure which confirmed C_{60} molecules were preferentially adsorbing to LL sites which were rich in nickel and cobalt, and forming chains in the periodic direction. This is not the one dimensional Fibonacci chain predicted, however it does show site specific adsorption of the C_{60} molecules onto the twofold surface of the quasicrystal Al-Ni-Co.

Contents

Declaration of Authorship i

Abstract iii

Contents vi

1 Introduction 1
- 1.1 Quasicrystals . . . 1
- 1.2 The Twofold Quasicrystalline Al-Ni-Co . . . 3
- 1.3 Surface Science . . . 4
- 1.4 C_{60} Deposition . . . 5

2 Method 7
- 2.1 Overview of Techniques . . . 7
  - 2.1.1 Ultra-High Vacuum . . . 7
  - 2.1.2 Surface Preparation . . . 8
  - 2.1.3 Scanning Tunnelling Microscopy . . . 9
  - 2.1.4 Data Analysis . . . 10
- 2.2 Experimental Details . . . 10
  - 2.2.1 Experiment . . . 10
  - 2.2.2 Analysis Method . . . 11

3 Results and Analysis 14
- 3.1 Clean Surface . . . 14
  - 3.1.1 Step Height . . . 14
  - 3.1.2 Relating Clean Surfaces Before and After Dosing . . . 16
  - 3.1.3 Surface Ordering . . . 18
- 3.2 C_{60} Adsorption . . . 20

4 Conclusion 24

References i

List of Figures ix

List of Tables **x**

Appendices **xi**

Appendix A Literature Review **xii**
A.1 Quasicrystals and Al-Ni-Co xii
A.2 Techniques and Requirements xiv
A.3 Deposition of C_{60} xvi

Appendix B Analysis **xx**
B.1 Step Height Example xx
B.2 Surface Ordering Example xxii
B.3 Relating Clean and Dosed Surfaces Example xxiii
B.4 Determining C_{60} Position Example xxviii

Chapter 1

Introduction

The aim of this project is to explore the growth of C_{60} on the twofold Quasicrystalline surface of Al-Ni-Co using scanning tunnelling microscopy (STM). This chapter serves as an introduction to the project as well as a short summary of the underlying physics. For further background information, see the literature review in appendix A. This project involved the preparation of the sample, analysis and characterisation of the surface and the deposition of C_{60} onto it. Details of the methods and analysis undertaken are described in chapter 2, the results are shown and discussed in chapter 3.

1.1 Quasicrystals

Quasicrystals were first observed by Dan Shechtman in 1984 [1], with the discovery earning him the Nobel Prize in Chemistry in 2011. Quasicrystals are structures which are ordered and have symmetry but do not possess translational periodicity, such as one would expect from a conventional crystal. The structures often possess symmetries traditionally forbidden by periodic or Bravais lattice systems, such as five- or tenfold.

Translational periodicity is where an atom or group of atoms (known as a basis) resides at each vertex point in a periodic lattice, giving repeating identical segments which are related by R, the lattice vector:

$$\mathbf{R} = n_1\mathbf{a_1} + n_2\mathbf{a_2} + n_3\mathbf{a_3} \tag{1.1}$$

Where n_1, n_2, n_3 are arbitriarty integers and $\mathbf{a_1}, \mathbf{a_2}, \mathbf{a_3}$ are the lattice vectors in 3D. These periodic structures can only possess one–, two–, three–, four–, and sixfold symmetries as other rotations do not result in a crystal with every point of the body coincident with an equivalent point of the object in its original orientation [2].

Conversely, long range aperiodicity is typical of quasicrytals. One way the quasiperiodic strucutre can be ordered is based on the Fibonacci sequence, such is the case for the twofold Al-Ni-Co quasicrystal sample used in this project. The Fibonacci sequence of numbers is where each number in the sequence is the sum of the two preceding numbers. The one dimensional Fibonacci chain can be generated using short (S) and long (L) sections with substitution rules of $S \rightarrow L$ and $L \rightarrow LS$ [3] which will generate aperiodic order:

$$\begin{gathered}(1)L \\ (2)LS \\ (3)LSL \\ (4)LSLLS \\ (5)LSLLSLSL...\end{gathered} \tag{1.2}$$

The ratio of the long to short segments is

$$L = \tau S \tag{1.3}$$

Where τ is an irrational number, termed the golden mean:

$$\tau = \frac{1+\sqrt{5}}{2} \tag{1.4}$$

The surface used in this project is twofold, meaning that its atomic rows are arranged in a Fibonacci sequence. In the Fibonacci sequence, it is possible to have a chain of LL (two long segments) or LS (one long segement and one short) but two short segments (SS) is not permitted [4]. An example of the one dimensional Fibonacci chain made up of long and short sections is shown in figure 1.1.

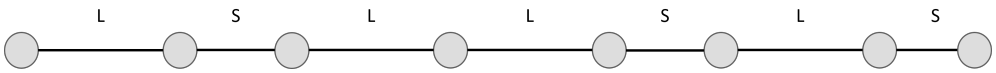

Figure 1.1: A section of the one dimensional Fibonacci chain composed of long (L) and short (S) sections. In terms of this project, the circles represent atoms and the lines represent the spacing between them.

1.2 The Twofold Quasicrystalline Al-Ni-Co

The Al-Ni-Co quasicrystal has both tenfold and twofold symmetries, which lie in perpendicular directions. In this project the twofold surface is considered, which is characterised by its unusual structure: it has a periodic direction which is perpendicular to the quasiperiodic direction. The distance between atoms in the periodic direction has been found to be close to 2 Å. The aperiodic spacing has is characterised by its distinct quasiperiodic ordering in the form of a one dimensional Fibonacci chain, with short and long sections which have been shown to be close to 5 Å and 8 Å respectively [5,6]. The τ relation between the long and short section is important in proving this Fibonacci

A model of the structure used in this project has been provided, which has been analysed in VESTA [7]. The surface which is imaged by STM is shown in figure 1.2 and the step heights between terraces are shown in the model in figure 1.3.

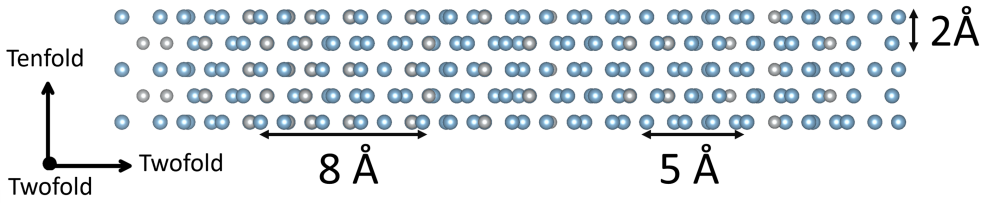

Figure 1.2: Model showing the periodic atomic spacing (2 Å) in the tenfold direction and the quasiperiodic atomic spacing (5 Å and 8 Å) in the twofold direction for the twofold surface of Al-Ni-Co. The blue represents aluminium and the grey represents the transmission metals nickel and cobalt.

The model shown in figure 1.2 was used to determine the expected atomic spacing for this precise composition. The expected periodic spacing (tenfold direction in the model) and the quasiperiodic spacing (twofold horizontal direction in model) is shown in table 1.1. The model in 1.3 was used to extract the expected step height between terraces, with the expectcted values shown in table 1.2.

Spacing	Distance (Å)
Periodic	2
Short	5
Long	8

Table 1.1: The periodic, long and short atomic distances as calculated from the model (figure 1.2).

From this model it was predicted that C_{60} would adsorb in a way which mimics the surface (templated growth), forming a one dimensional Fibonacci grid overlayer.

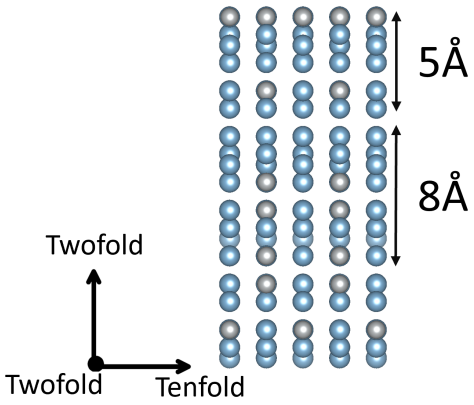

Figure 1.3: Model showing the separation of similar high density atomic planes in the twofold direction (5 Å and 8 Å). The blue represents aluminium and the grey represents the transmission metals nickel and cobalt.

Type of Step	Step height (Å)
Short	5
Long	8

Table 1.2: The expected step heights between terraces from the model (figure 1.3).

1.3 Surface Science

In order to understand the processes involved in this project, a background understanding of surface science is required. Surfaces are formed through the breaking of bonds and thus, surface atoms have fewer neighbouring atoms than the bulk. Therefore, these surfaces have a state of elevated energy and enhanced chemistry. Impurities on the surface can modify the physical and chemical properties of a material and change the arrangement of the atoms [8]. Hence, it is essential that the surface used in this project is clear of impurities and defects.

The surfaces of crystals have terraces (flat regions) and defects (such as steps, kinks or point detects). The crystal surface can be described as flat if the ratio of terrace to defect sites is high. These defect sites have a different atomic environment as well as different electronic and chemical properties. The number of defects depends heavily on the surface orientation, the preparation methods and on whether there are any vacancies in the bulk.

As atoms at the surface have a smaller coordination number (are bonded to fewer ions) compared to the bulk, in order to maximise the coordination, the surface atoms

rearrange, developing a new equilibrium position and giving the surface different properties to the bulk. This rearrangement occurs either through surface reconstruction or surface relaxation. Surface reconstruction is the process where the surface atom shifts parallel to the surface which can change the periodicity [9]. This can result in missing individual atoms or even whole rows in comparison to the bulk. Surface relaxation involves the compression and extension of the top interlayer separation normal to the surface [10]. The first layer of atoms contract towards the second layer, increasing their coordination. This causes the third layer of atoms to move away from the second layer to compensate the over coordination of the second layer. This oscillation in layer separation penetrates five to six layers from the top in a region called selvedge. The surface symmetry is not changed by relaxation [11].

Under suitable preparation, quasicrystals can give atomically flat terraced surfaces, characteristic of bulk truncations [12]. The quasicrystal surface corresponds to bulk truncations at the positions where blocks of atomic layers are separated by larger interlayer spacings [13]. The symmetry of the bulk is retained at the surface, with diffraction patterns of topmost layers being consistent with those of the bulk terminated surface [14].

1.4 C_{60} Deposition

Quasicrystals make interesting substrates as they have unusual but distinctive environments which give different adsorption landscapes compared to crystalline materials [15]. The way in which the adsorbates arrange themselves on the quasicrystals provides insight into the quasicrystal surface structure and chemistry. Monolayers of Bi and Sb have been found to adopt the substrate structure of decgonal Al-Ni-Co [16], and thus, there is interest in exploring the adsorption of C_{60}. The aim of this project relies on a unique adsorption-site network where there is a strong enough molecule-surface interaction for C_{60} films to grow in a quasicrystalline manner rather than in close packed crystalline field [17, 18]. Generally, C_{60} grows in a close-packed hexagonal fashion [19]. Growing a quasicrystalline C_{60} layer would be in contrast to the self-assembled C_{60} layers on periodic crystalline surfaces.

C_{60} has been chosen for adsorption onto the quasicrystal surface as it has a number of favourable properties. The molecules behave isotopically and have two-, three-, and fivefold symmetries which match with the twofold surface used in this project. Symmetry matching is important as it has been shown to impact on the molecule-quasicrystal interaction [20, 21]. C_{60} molecules are further desirable in STM analyses

as they are large and isotropic making them easier to image. It is regularly used as an adsorbate as it is a good electron absorber [22] meaning a strong electronic molecule-substrate interaction is expected. Nickel is an electron-rich element, and thus it is expected that C_{60} will preferentially adsorb on these sites. Such site-specific adsorption has been shown previously for other surfaces [18,21,23] and so it is reasonable to predict similar results. Preferential adsorption is shown in figure 1.4, here C_{60} is adsorbed onto Al-Pd-Mn. This figure shows preferential adsorption of C_{60} onto the manganese atoms since manganese is electron rich [23].

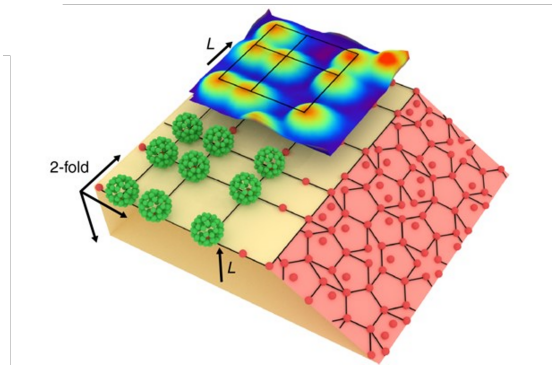

Figure 1.4: This schematic diagram shows the way in which C_{60} is expected to adsorb onto the quasicrystaline surface, with this schematic using the surface of Al-Pd-Mn as an example. STM images are overlayed to show relation between substrate and overlayer. The yellow represents the twofold orientation and the pink represents the fivefold orientation. The red dots correspond to Mn atoms, to which C_{60} (green) preferentially adsorbs. Image from [23].

Chapter 2

Method

This chapter describes the techniques employed throughout this project and the specific experimental method used. An overview of the techniques is found in section 2.1 and the experimental process followed in this project is described in section 2.2.

2.1 Overview of Techniques

This section serves as an overview of the techniques used, the reasoning behind their implementation, and any underlying physics.

2.1.1 Ultra-High Vacuum

In order for this project to be carried out successfully it is essential that the correct conditions are met, and the appropriate techniques, such as Ultra-High Vacuum (UHV) [24], are used. The sample was prepared under UHV conditions, generally defined as pressures below 10^{-8} mbar (with 10^{-10} mbar used in this project for sample preparation). This is to avoid any contamination of the surface from ambient gasses (for example oxidation), allowing the surface to be kept clean over the period of the experiment [25]. As this project uses an aluminium based sample, the surface will oxidise similarly to elemental aluminium, destroying the quasicrytalline surface. For this reason, it is important to provide an environment free from ambient gases.

Using UHV increases the mean free path of any electrons in the chamber as there are virtually no particles with which to collide, meaning that any interactions will be with the surface inside the UHV chamber. When the number of particles is reduced the interactions with the probe that could disturb the measurement become less likely.

UHV conditions are created and maintained using multiple pumps to remove undesired particle within the chamber [26].

2.1.2 Surface Preparation

The twofold quasicrystaline surface must be prepared properly in order to observe the quasiperiodic ordering and deposit C_{60}. The surface needs to be cleaned from any impurities or contaminants, such as oxygen. When exposed to air an oxide layer a few nanometres forms on the surface [27]. This layer of surface impurities must be removed and the surface needs to the expected structures. This was achieved through repeated rounds of sputtering and annealing.

Sputtering is the process of bombarding the surface with inert gas ions which are directed towards the sample, as shown in figure 2.1. The incident ions eject chemisorbed and physiosorbed species from the surface alongside surface atoms. This process removes contamination but leaves a rough surface which is unsuitable for the experiment. The less bound surface atoms or lighter mass elements are ejected preferentially. When

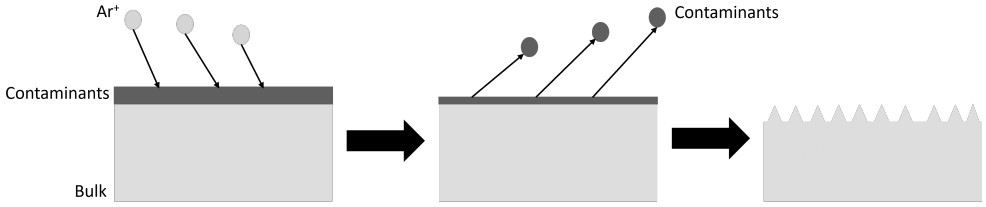

Figure 2.1: Diagram shows the process of sputtering. Ar^+ ions are incident on the surface and removes the contamination, leaving a rough surface.

such a process is performed on a quasicrystal, a crystalline phase is created through this change in stoichiometry [14, 28].

In order to achieve an atomically flat quasicrystalline surface the sample was annealed by heating to a high temperature, as shown in figure 2.2. This provides enough thermal energy for surface atoms to diffuse from bulk to the surface, replenishing any atoms preferentially removed during sputtering.

The annealing process also removes any sputtered ions which adsorbed to the surface. Through heating, energy is provided to the bulk of the sample allowing it to reach a state closer to equilibrium, return to a quasicrystalline structure, and form terraces (flat regions on the surface separated by a change in height). Careful selection of the annealing temperature is critical as it must provide enough energy without melting the sample. The process of determining the annealing temperature is discussed further in

the literature review (appendix A) and in the data acquisition section (section 2.2). Repeated cycles of sputtering and annealing are used to create a flat, ordered surface which is suitable for structural analysis and adsorption studies.

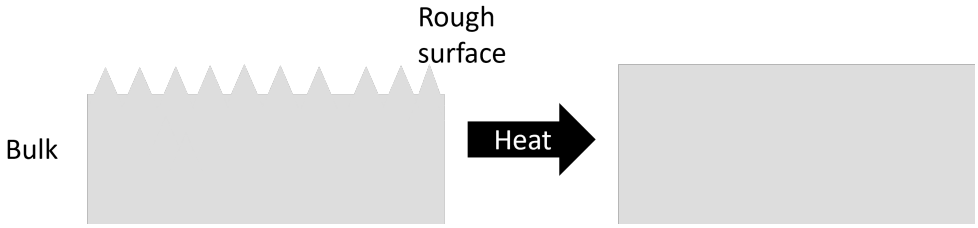

Figure 2.2: Diagram shows the process of annealing. The surface is heated and becomes flat. Through providing energy to the bulk the surface reaches a state closer to equilibrium.

2.1.3 Scanning Tunnelling Microscopy

The main technique used in analysis for this project is Scanning Tunnelling Microscopy (STM). This technique which was discovered by Binnig and Rohrer [29] in 1982. It is widely used to observe the surfaces of materials as it allows for the imaging of individual atoms or molecules [30]. STM achieves a high spatial resolution using the quantum phenomenon of electron tunnelling. An extremely sharp tip with a bias voltage applied is brought close to the surface of the sample. The potential difference between the tip and the surface allows electrons to tunnel between the two materials, as seen in figure 2.3. A tunnelling current arises, which depends exponentially on the distance between

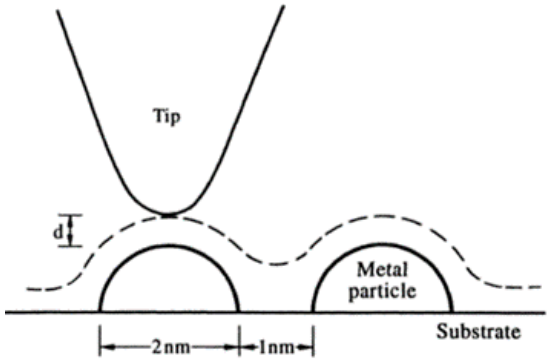

Figure 2.3: A schematic of the path the STM tip takes as it measures d, the distance between the tip and the surface. This diagram shows observation of ultra fine metal particles in the constant current mode. Image from [30].

the tip and the surface. This relationship is very sensitive as a distance change of 1

Å can cause an order of magnitude difference in the tunnelling current [31]. Through measuring this, the topography of the sample can be mapped, allowing for the surface to be imaged [32]. The lateral resolution is dependent on the size of the tip and so a fine tip is key to achieving good resolution. When using STM, careful analysis is essential as protrusions observed on the surface could be topographical or due to an increase in the local density of states.

STM has been used widely in the study of quasicrystals [33], with the first example for the twofold surface of quasicrystalline Al-Ni-Co, done by Kishida et al. [5]. The technique used in this project was constant current mode. This technique moves the tip vertically in order to maintain a constant current between the tip and sample. The voltage required to move the tip was measured and thus related to the changing height of the tip.

2.1.4 Data Analysis

The STM data was processed using WSxM [34]. This is a program that allows for manipulation of STM images. It was used to flatten the images, read the changes in height recorded through STM, and measure lateral distances. The tip and sample are never truly perpendicular, which can give uneven heights across the scan. This creates an image that does not match the flat surface of the sample. Plane levelling corrects these discrepancies by flattening the images to be more representative of the true structure.

2.2 Experimental Details

This section details the method used for data gathering and analysis for this project.

2.2.1 Experiment

The crystal was grown by Peter Gille (Ludwig Maximilian University of Munich) using the Czochralski method [35], as described in reference [36], but with a different melt. The composition of the sample is $Al_{71.8}Ni_{14.6}Co_{13.4}$ [37]. The sample was polished and care was taken to ensure that no one orientation was polished favourably. The quasicrystal was then mounted onto the centre of a sample plate using tantalum wire and placed inside the UHV chamber. The plate was heated from the centre and so the central position in aided the heating process and prevented the sample from cooling too quickly – which could have damaged it. The sample was prepared through sputtering

and annealing with annealing temperature between 650 °C and 700 °C (as determined from the literature review in appendix A), with a preferred preparation chamber pressure of $10^{-10} - 10^{-9}$ mbar. Ar^+ was used for sputtering with a drain current of around 4.5 μA and the sample was annealed for sessions of 1-3 hours. Throughout the preparation process the surface ordering and cleanliness were monitored using STM. The surface was determined to be ready when there were clear terraces and good resolution.

Clean surface STM images were taken for later analysis before the sample was dosed with C_{60}. The C_{60} molecules were evaporated in-situ by applying current through a tungsten filament tightly wound around the Pyrex tube in which the powder was contained. The C_{60} coverage was built up over multiple bursts and it was found that depositing with the surface at a higher temperature (300°C) provided the best results. This is because the increased temperature allowed the molecules to diffuse and select an equilibrium site, binding to the surface at these preferred sites. STM images of the dosed surface were taken and these are shown, along with the clean surface, in chapter 3.

2.2.2 Analysis Method

Step Height Analysis

In order to confirm the quasicrystalline nature of the surface, the step heights between the terraces were quantified and analysed. Clean surface images with clear terraces were selected, areas of the same height were flattened and the step heights between the terraces were measured. These terrace heights were recorded, and the frequency of different step heights were assessed, with expected step heights of 5 Å (S) and 8 Å (L) (and combinations of these heights). Some step heights were smaller than expected and these were determined to be incomplete terraces, termed 'half steps'. When such a step was recognised, it was removed from analysis, however, due to limited resolution not all were able to be identified. An example of this analysis can be found in appendix B.1 and the results of this can be found in section 3.1.

Relating Clean Surfaces Before and After Dosing

This area of analysis involved relating the clean surface before and after dosing by comparing the measured distances between atomic rows on both surfaces. 'Clean' refers to areas of the surface without C_{60} adsorption. For various sections of the given surface, the middle of each visible atomic row was identified through a line profile and visual

analysis of the STM image. The separation between these row centres were measured from the line profile. Spacings of each type were averaged for each surface. The clean areas after dosing were analysed first as this surface was imaged with a higher resolution. This allowed for more reliable and detailed measurements. The surface before dosing was then analysed in the same manner, however, the poor resolution made it difficult to identify individual L and S distances – thus L+S combinations were the focus of the following comparison. The averages across both surfaces were compared, allowing the surfaces to be related.

had been imaged with a higher resolution, and thus they were used as a baseline for comparison with the surface before dosing. Distances were measured at various positions across the dosed surface and average distances for L, S and combinations were found. Once this was complete for the surface after dosing, this was then done for the images of the surface before dosing, and related to the results previously found. Due to poor surface resolution, L+S combinations were easier to observe and thus were the focus of this analysis.

This analysis was important as similar surface structure would indicate that the model provided is valid for the dosed surface. This was essential in characterising the C_{60} adsorption. An example of this analysis can be found in appendix B.3 and the results are shown in section 3.1.2.

Surface Ordering

To understand the surface, the distances between atomic rows were measured to characterise the quasiperiodicity. For the surface before and after dosing, the distances between the atoms in the periodic direction (expected 2 Å) and quasiperiodic (expected 5 Å and 8 Å) were measured. The occurrences of each distance was recorded in order to compare the clean to the dosed surface and the averages were taken.

This analysis was essential to the next steps as the results could then be used to determine where the C_{60} adsorbed and if there was any relation in its position to the substrate. An example of this analysis is in appendix B.2 and the results can be found in section 3.1.3.

Positions of C_{60} Adsorption

The dosed surface was analysed by searching for patterns and repeated motifs. Any areas of interest were analysed using the line profile tools and used to determine where on the substrate C_{60} tended to deposit. This was then related to the model in order to

determine any preferred adsorption sites.

An example of this analysis is in appendix B.4 and the results are shown in section 3.2.

Chapter 3

Results and Analysis

This chapter contains the results after undergoing the experimental and analytical methods described in chapter 2. It also includes in depth discussion of these results.

3.1 Clean Surface

3.1.1 Step Height

Images of the clean surface before the dosing were used in analysis of the step heights, where the step height is the height difference between neighboring terraces. A step height measurement is shown in figure 3.1. The histogram was used to get the step

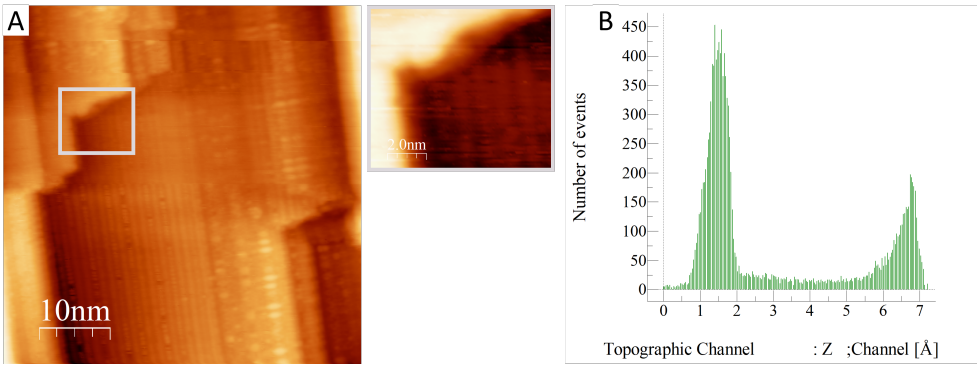

Figure 3.1: A: STM image of the clean surface with multiple clear terraces. An area that contains a change in terrace is highlighted. The highlighted area has been plane flattened to achieve the most accurate step height data. Figure B represents a histogram of the Z heights for figure A. It plots the frequency for each Z height, thus the peaks give the most common Z heights for the image. The step height is therefore measured as the difference in Z between the histogram peaks.

height as it plots the frequency of each Z height and the step height can be measured from the spacing between the peaks. For this example, the step was determined to be 0.534 nm.

This process was repeated for 29 steps across multiple images covering different areas of the surface. The full analysis over these steps is shown in figure 3.2, a histogram of measured step heights. This revealed clear peaks at common step heights corresponding to the expected S and L heights. The average step height for long and short steps are summarised in table 3.1.

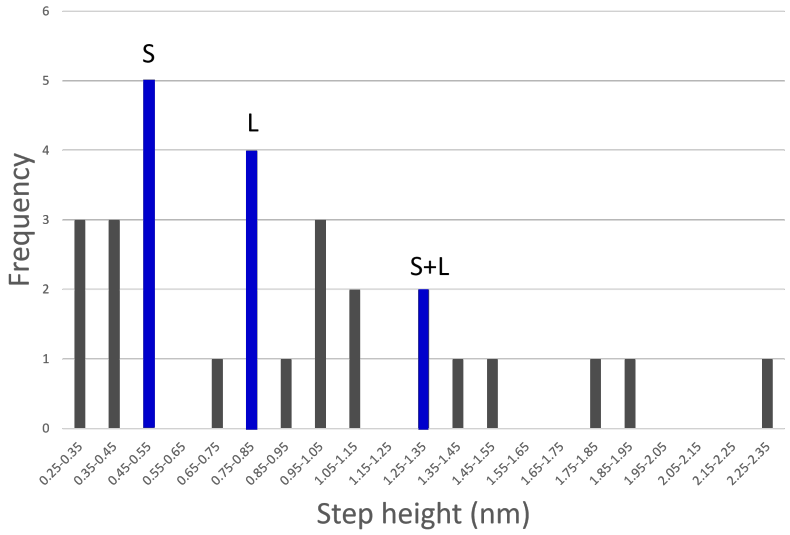

Figure 3.2: Histogram showing the frequency of given step heights for the clean surface. There are clear peaks at 5 Å and 8 Å.

Type of Step	Average Height (nm)
S	0.517 ± 0.02
L	0.827 ± 0.02

Table 3.1: The average step height measured for the short (S) and long (L) steps. The errors were determined from the spread of the values measured.

Some smaller steps were noted which appeared to be from incomplete steps (an example of this is in appendix B.1). Due to limited resolution not all of these were able to be identified, and thus, it is assumed that the majority of outliers can be attributed to these incomplete steps. The presence of not fully steps could indicate the annealing temperature was too low, however increasing this would have risked melting the surface. Other outliers were due to issues with image resolution or caused by the surface not

being entirely uniform and thus, may not have adopted a quasicrystalline structure during annealing. As well as the expected S and L steps there are also clear peaks at combinations, such as around 13 Å (S+L). A bin size of 1 Å was chosen so as to allow for any errors in the measurements.

Throughout the 29 steps analysed, two L steps in a row were observed as well as LS, but SS did not appear. This is consistent with the Fibonacci sequence as described in section 1.2, as an SS chain is forbidden. The clear peaks at the expected step heights between the terraces (summarised in table 3.1) and the order in which they occur, show the surface was quasicrystalline, with the L and S step heights being consistent with the model, as expected.

3.1.2 Relating Clean Surfaces Before and After Dosing

The surface was successfully prepared and all contamination was removed, with clear terraces forming after the sputtering-annealing process. The surfaces before and after dosing were clearly imaged by STM with rows and terraces visible. The images before dosing do not have atomic resolution and thus appear to be of poorer quality. This is partially due to issues with the tip and any roughness of the area being imaged. Example images of both surfaces are shown in figure 3.3. Here it is clear that the images of the clean surface before dosing have lower resolution.

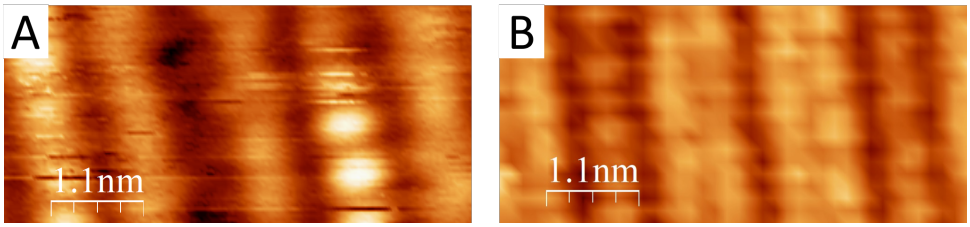

Figure 3.3: STM images of the clean surface covering areas of the same size. A shows the surface before dosing, B shows the clean surface after dosing. Both images have been plane flattened. The surface before dosing does not show atomic resolution unlike the surface after dosing. There are fewer rows visible in the surface prior to dosing, with only those especially bright discernible.

The surfaces were characterised through measuring the interatomic spacing between rows and relating the surface before dosing to the clean surface after. The surface after dosing was characterised first, as it had atomic resolution (as demonstrated in figure 3.3). The surface was characterised as shown in figure 3.4 A, with S and L distances overlayed. This shows the expected order of L and S across the surface in

the quasiperiodic direction. This was then used to similarly characterise the surface before dosing, as seen in figure 3.4 B. Here, the distances were only able to be measured between the bright rows, which were apparent even with poorer overall resolution. For this reason, combinations of L and S were necessary to relate the surfaces. This issue with the image quality also meant that the measurements on the undosed surface were less precise.

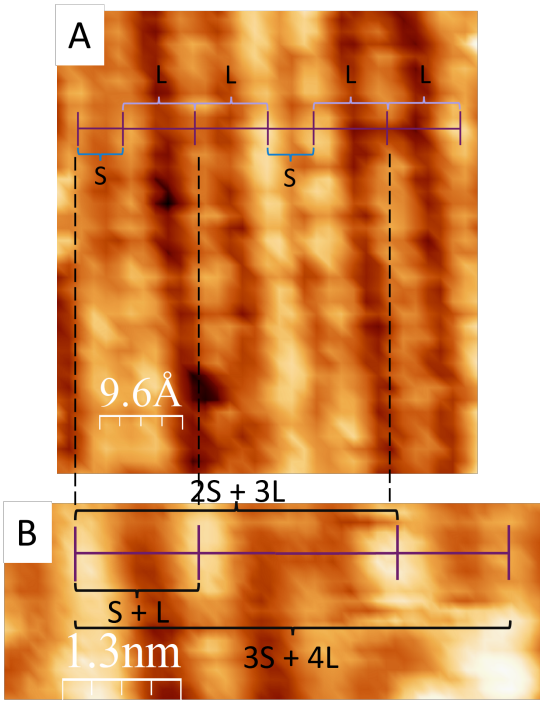

Figure 3.4: A: an STM image of the clean part of the surface after dosing which has a ruler with the short and long atomic spacings overlayed. B: The clean surface before dosing, with a ruler overlayed showing the spacing present on the surface. Here the average long and short values were used (as described in section 3.1.3), with $S = 0.525$ nm and $L = 0.768$ nm. The dashed lines connects the segments between the two surfaces.

From these comparisons, the clean surface before and after dosing were able to be related and confirmed to exhibit the same quasiperiodic ordering. Both surfaces demonstrate the same long and short sections and the relation between them is exemplified in figure 3.4. From this analysis it is clear that the clean surfaces before and after dosing can be related to each other in terms of the quasiperiodic long and short spacing.

3.1.3 Surface Ordering

Multiple images were used to collect a large quantity of interataomic distances: for the clean surface before dosing 61 distances were measured in the periodic direction and 59 in the quasiperiodic, for the surface after dosing 29 were measured in the periodic direction and 48 in the quasiperiodic direction. These distances were then grouped into bins of 1 Å, in order to create a set of histograms.

The periodic atomic distances for clean surfaces before and after dosing are shown in figure 3.5. For both surfaces there are clear peaks at distances of 2 Å and multiples of 2 Å, as expected. The average periodic atomic spacing for both surfaces are summarised in table 3.2.

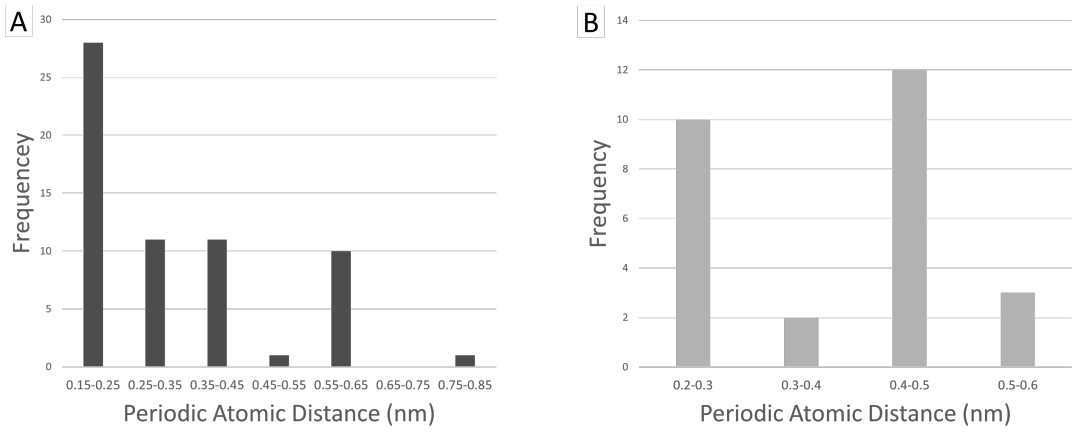

Figure 3.5: A: the frequency of atomic distances along the periodic direction for the surface before dosing. B the frequency for the substrate after dosing. There are clear peaks at the expected 2 Å and multiples of 2 Å.

Surface	Average Distance (nm)
Before Dosing	0.198 ± 0.01
After Dosing	0.221 ± 0.02

Table 3.2: The average periodic atomic distances for the surface before and after dosing. The errors were determined from the spread of the values measured.

The results for the quasiperodic distances are shown in figure 3.6. There are clear peaks around 5 Å and 8 Å for both surfaces, as expected, as well as notable peaks at L+S combinations for the surface before dosing. The average atomic distances for short and long spacings for both surfaces are described in table 3.3.

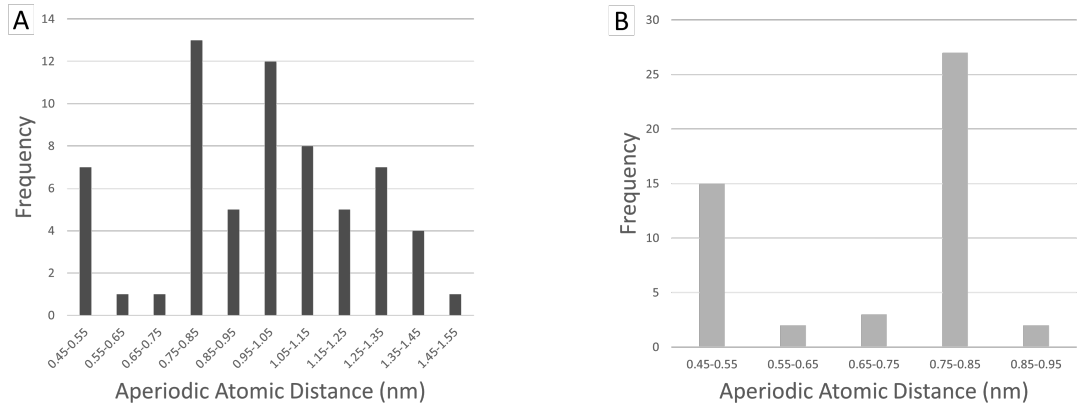

Figure 3.6: The frequency of aperiodic atomic distances for the clean surface before dosing (A) and after dosing (B).

Spacing	Average Distance (nm)	
	Surface Before Dosing	Surface After Dosing
S	0.520 ± 0.02	0.510 ± 0.02
L	0.800 ± 0.02	0.803 ± 0.02

Table 3.3: The average aperiodic atomic distances (S and L) for the clean surface before and after dosing. The errors were determined from the spread of the values measured.

Analysis of the surface atomic ordering showed that the periodic spacing was found in the vertical direction and quasiperiodic in the horizontal direction, as shown in the model in figure 1.2. This is consistent across all STM images of the surface.

As previously discussed, the images of the clean surface before dosing did not have atomic resolution, thus the distances measured are less precise than the clean surface after dosing, for which images with atomic resolution were obtained. Hence, images of the surface prior to dosing exhibits a higher number of peaks that do not fit the expected interatomic spacing. In the periodic direction there were clear peaks at the expected 2 Å and at multiples of this distance for both surfaces. For both surfaces, the average periodic atomic distance was consistent with expectations provided by the model.

In the quasiperiodic direction, the clean surface after dosing showed clear peaks at the expected distances. As discussed above, the surface before dosing provided poorer quality images, however peaks are still observed at the expected long and short distances. The poor resolution meant combinations of long and short distances were

measured as it was too challenging to resolve many single L and S distances. The average distances found for the periodic and quasiperiodic directions are in line with each other for both surfaces and strongly agree with the model and the literature.

This shows that both surfaces (before and after dosing) match well with expectations, showing clear periodic spacing in one direction and quasiperiodic spacing in the perpendicular direction. The distances are consistent between the two surfaces and align well with the predicted values.

3.2 C_{60} Adsorption

The dosed surface exhibits good coverage of the deposited C_{60} as well as atomic resolution of the substrate. Around 20% of the surface was covered, allowing for ample C_{60} to analyse and enough substrate visible for relating to the images of the surface prior to dosing.

On the dosed surface, motifs of C_{60} adsorption were noted. One such motif was a repeated pattern of two C_{60} molecules deposited close together, which was termed a 'thumbprint'. The frequency of this is shown in figure 3.7, where these thumbprints are highlighted.

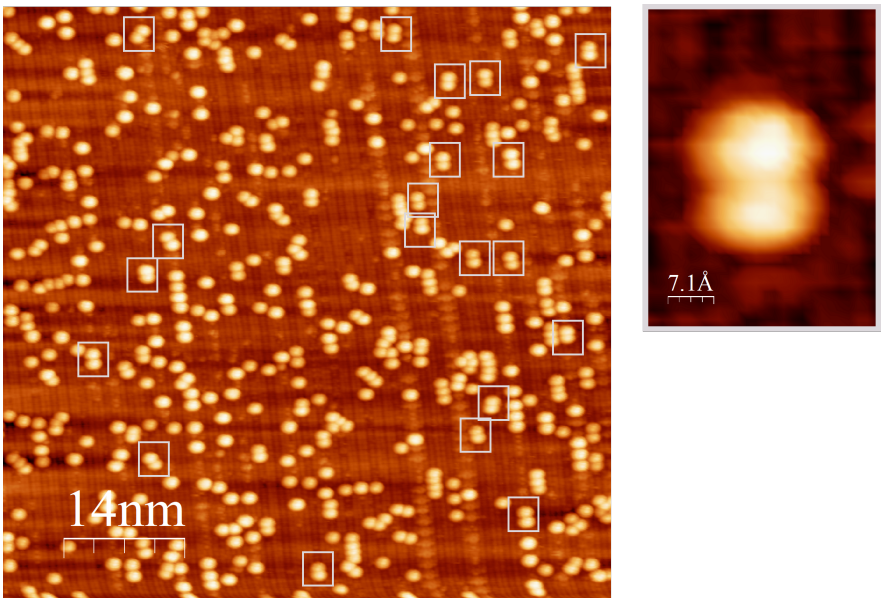

Figure 3.7: The dosed surface with instances of the two C_{60} molecule (thumbprint) motif highlighted with an enlarged example of one such 'thumb print'.

These thumbprints were selected and the surrounding clean surfaces were analysed,

demonstrated in appendix B.4. This found that the C_{60} deposited between two long sections on the surface (with long sections defined as in section 3.1.3), termed 'LL' sites. From observation of the dosed surface, two kinds of sites were apparent: 'light', where the substrate surrounding the C_{60} was light in colour (figure 3.8), and 'dark', where the substrate surrounding the C_{60} showed darker contrast (figure 3.9).

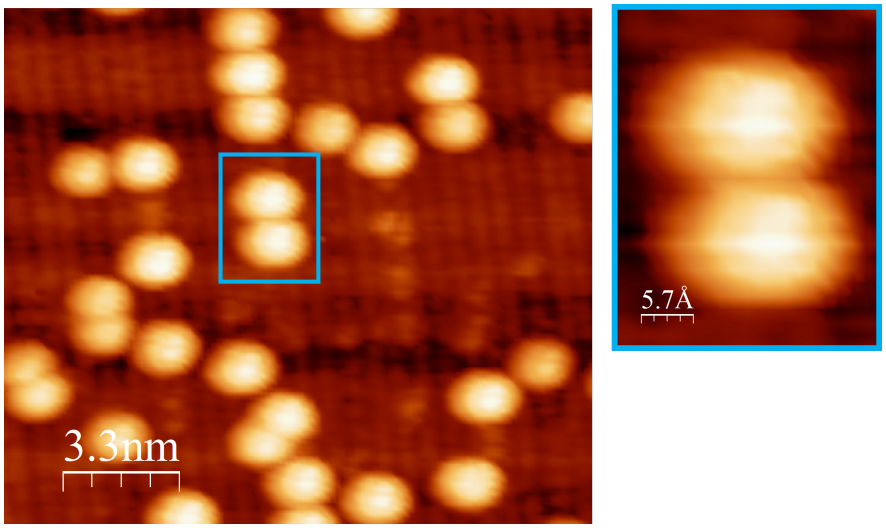

Figure 3.8: An example of a light C_{60} adsorption site is highlighted. The substrate surrounding the site is shown to be lighter in colour.

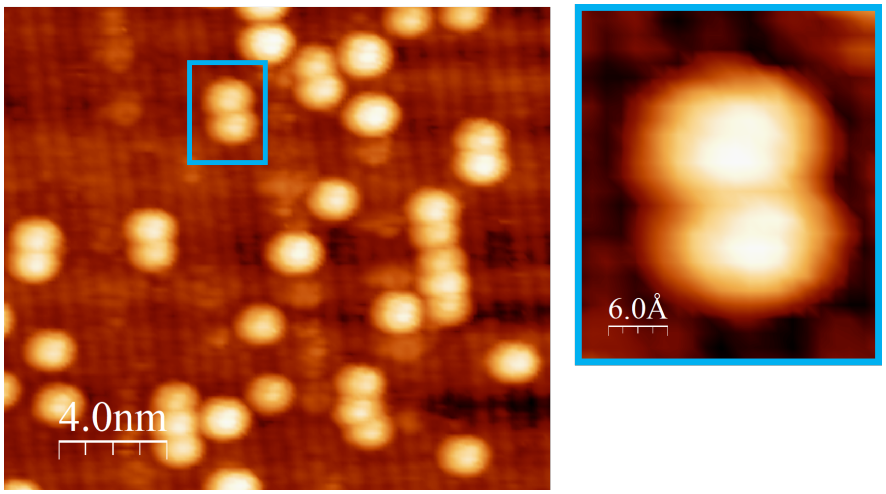

Figure 3.9: An example of a dark C_{60} adsorption site is highlighted. The substrate surrounding the C_{60} is notably darker than in figure 3.8.

The difference between the light and dark sites appears to be due to a change in

height, with the maximum height of the C_{60} on the light site being 1 Å higher than the dark. This was caused by the different positions and height of nickel and cobalt atoms at these sites. The fact that the dark sites are lower and yet still have C_{60} adsorption shows the bonding molecule-substrate interaction is strong enough to have adsorption on both site types. This knowledge allowed for such sites to be found on the model, allowing for better understanding why the C_{60} molecules appear to preferentially adsorb in these areas.

Another notable motif was that of three to four C_{60} molecules adsorbing in a chain in the periodic direction, as shown in figure 3.10. As these molecules are following the periodic direction, it implies preferential adsorption to a particular site in the quasiperiodic direction. This was explored through modelling.

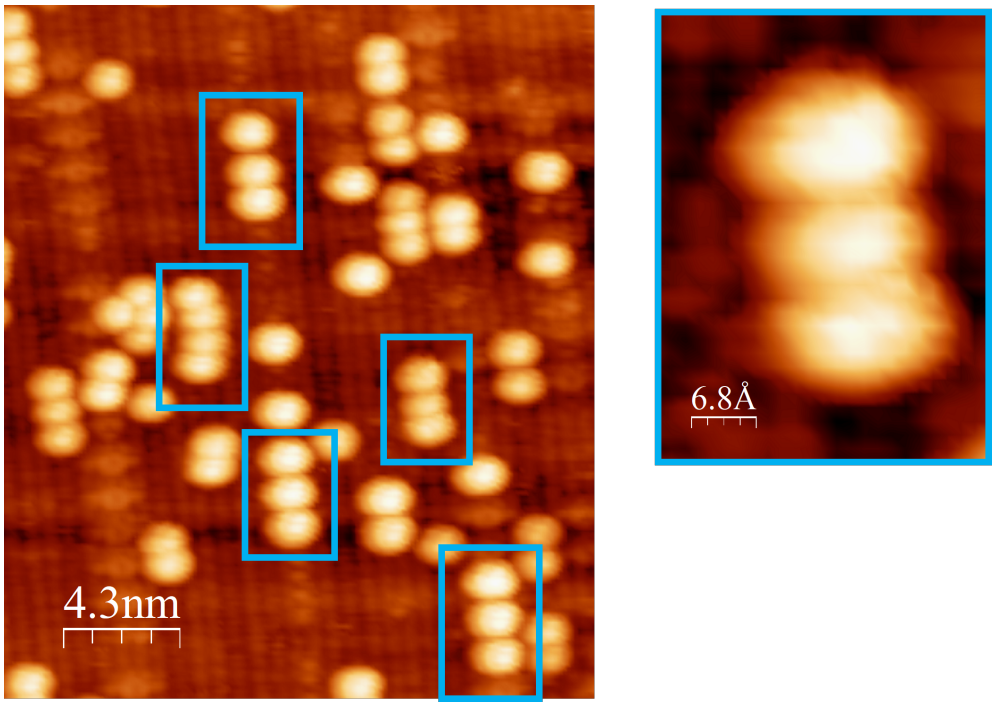

Figure 3.10: Three to four C_{60} molecules adsorbed in a chain in the periodic directions are highlighted, with one example enlarged.

When inspecting a high density plane of the model, it became possible to relate the C_{60} deposited on the surface to positions in the model. This was done for the chain motif shown in figure 3.10, modelled in figure 3.11.

From this it is apparent that C_{60} is preferentially adsorbing on LL sites that have high concentrations of nickel and cobalt compared to the majority of the structure. This is consistent with the understanding that C_{60} preferentially adsorbs to electron

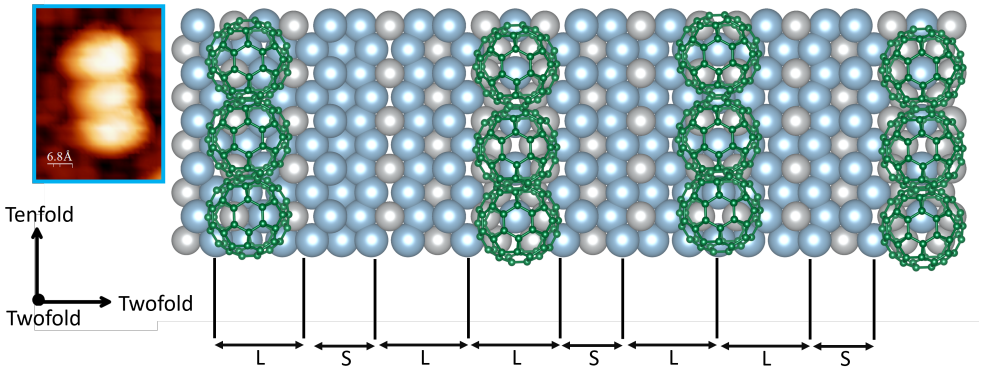

Figure 3.11: Possible adsorption sites for the chain motif (as seen in figure 3.10) on the model with an STM example of the motif alongside. The model shows the periodic and quasiperiodic directions aligning with the vertical and horizontal directions respectively. In the model, the green represents the C_{60}, the blue represents aluminium atoms and grey represents nickel and cobalt atoms. The long and short spacings are labelled, with the C_{60} shown to adsorb in the LL sites.

rich elements.

From observation of the dosed surface in figure 3.7, it is clear that the C_{60} molecules have diffused and deposited across the surface in a non-arbitrary fashion. There are repeated motifs found in the deposition, especially in the periodic direction, suggesting that the molecules have adsorbed to the same type of spacing in the quasiperiodic direction, LL. Through this analysis it has been determined that these C_{60} molecules preferentially adsorb on LL sites. This was explored further by finding appropriate areas in the model onto which C_{60} could adsorb. These areas were confirmed to be nickel and cobalt rich, reinforcing the hypothesis that C_{60} preferentially adsorbs to these electron rich elements. It currently unclear why LL sites are preferred, a potential solution being that these sites provide the molecules with enough space. C_{60} is a large molecule, just under 1 nm in diameter, and thus adsorbing between long segments may be more favourable.

Chapter 4

Conclusion

This project has been successful in investigating the growth of C_{60} molecules on the twofold surface of the Al-Ni-Co quasicrystal. The surface was prepared effectively, dosed and imaged via STM. Through analysis of the step heights between terraces the surface was determined to be quasicrystalline in the direction normal to the surface, forming a quasiperiic sequance of short and long steps related by τ (the golden mean). This was further demonstrated when the average atomic spacings were determined for both the periodic and the quasiperiodic direction. These results were consistent the literature and the model. This information was then used in determining preferential C_{60} adsorption sites.

The dosed surface showed a good coverage of C_{60} on the substrate, where the adsorption of C_{60} was deemed to be non-arbitrary and thus indicates preferential adsorption. Through analysis of the STM images and comparison to the model it was determined that C_{60} preferentially adsorbs onto LL sites that have a high nickel and cobalt concentration compared to the rest of the structure and, where possible, the molecules form a chain in the periodic direction. This is consistent with expectations as C_{60} is a good electron absorber, and nickel and cobalt are electron rich elements, making adsorption on these atoms favourable. Two kinds of LL sites were observed: light and dark, with a slight height difference between the two. This variation was believed to be caused by differences in the positions of nickel and cobalt, with thes positions being lower and producing a darker contrast. The C_{60} was not found to create a one dimensional Fibonacci chain as expected, but it has shown preferential adsorption in the periodic direction of a quasicrytalline surface, specifically on LL sites rich in nickel and cobalt. This evidence of preferential adsorption is important in furthering understanding of the interactions between C_{60} and quascrystalline substrates.

This was the first instance of C_{60} adsorption onto the twofold surface of the Al-Ni-Co quasicrystal and has thus opened up areas of future research. Further work is required into determining the orientation of the C_{60} molecules, as discerning which face adsorbs to the surface will provide information about the electronic interaction between the molecule and the substrate. Furthermore, investigation into an differences in the bonding for light and dark sites would be insightful into the electronic interactions between substrate and adsorbate.

Bibliography

[1] D Shechtman, I Blech, D Gratias, and JW Cahn. Metallic phase with long-range orientational order and no translational symmetry. *Physical review letters*, 53(20):1951, 1984.

[2] Michael Glazer, Gerald Burns, and Alexander N Glazer. *Space groups for solid state scientists*. Elsevier, 2012.

[3] Sam Coates. *Quasicrystal systems with simple symmetries*. The University of Liverpool (United Kingdom), 2019.

[4] Ron Lifshitz. The square fibonacci tiling. *Journal of alloys and compounds*, 342(1-2):186–190, 2002.

[5] M Kishida, Y Kamimura, R Tamura, K Edagawa, S Takeuchi, T Sato, Y Yokoyama, JQ Guo, and AP Tsai. Scanning tunneling microscopy of an al-ni-co decagonal quasicrystal. *Physical Review B*, 65(9):094208, 2002.

[6] JY Park, DF Ogletree, M Salmeron, RA Ribeiro, PC Canfield, CJ Jenks, and PA Thiel. Atomic scale coexistence of periodic and quasiperiodic order in a 2-fold al-ni-co decagonal quasicrystal surface. *Physical Review B*, 72(22):220201, 2005.

[7] Koichi Momma and Fujio Izumi. Vesta 3 for three-dimensional visualization of crystal, volumetric and morphology data. *Journal of applied crystallography*, 44(6):1272–1276, 2011.

[8] Franco Bassani, Gerald L Liedl, and Peter Wyder. Encyclopedia of condensed matter physics. 2005.

[9] Klaus Wandelt. *Encyclopedia of interfacial chemistry: surface science and electrochemistry*. Elsevier, 2018.

[10] Émilie Gaudry. 3.05 - an introduction to the theory of inorganic solid surfaces. In Jan Reedijk and Kenneth R. Poeppelmeier, editors, *Comprehensive Inorganic Chemistry III (Third Edition)*, pages 74–104. Elsevier, Oxford, third edition edition, 2023.

[11] Hans Lüth. *Solid surfaces, interfaces and thin films*, volume 4. Springer, 2001.

[12] Thomas M Schaub, Daniel E Bürgler, HJ Güntherodt, and JB Suck. Quasicrystalline structure of icosahedral al 68 pd 23 mn 9 resolved by scanning tunneling microscopy. *Physical review letters*, 73(9):1255, 1994.

[13] HR Sharma, Vincent Fournée, M Shimoda, AR Ross, Thomas A Lograsso, AP Tsai, and A Yamamoto. Structure of the fivefold surface of the icosahedral al-cu-fe quasicrystal: Experimental evidence of bulk truncations at larger interlayer spacings. *Physical review letters*, 93(16):165502, 2004.

[14] HR Sharma, M Shimoda, and AP Tsai. Quasicrystal surfaces: structure and growth of atomic overlayers. *Advances in Physics*, 56(3):403–464, 2007.

[15] R McGrath, JA Smerdon, HR Sharma, Wolfgang Theis, and J Ledieu. The surface science of quasicrystals. *Journal of Physics: Condensed Matter*, 22(8):084022, 2010.

[16] KJ Franke, HR Sharma, W Theis, P Gille, PH Ebert, and KH Rieder. Quasicrystalline epitaxial single element monolayers on icosahedral al-pd-mn and decagonal al-ni-co quasicrystal surfaces. *Physical review letters*, 89(15):156104, 2002.

[17] William IF David, Richard M Ibberson, Judy C Matthewman, Kosmas Prassides, T John S Dennis, Jonathan P Hare, Harold W Kroto, Roger Taylor, and David RM Walton. Crystal structure and bonding of ordered c60. *Nature*, 353(6340):147–149, 1991.

[18] JA Smerdon, KM Young, M Lowe, SS Hars, TP Yadav, D Hesp, VR Dhanak, AP Tsai, HR Sharma, and R McGrath. Templated quasicrystalline molecular ordering. *Nano Letters*, 14(3):1184–1189, 2014.

[19] Jules A Gardener, George Andrew D Briggs, and Martin R Castell. Scanning tunneling microscopy studies of c60 monolayers on au (111). *Physical Review B*, 80(23):235434, 2009.

[20] PJ Nugent, JA Smerdon, R Mcgrath, M Shimoda, C Cui, AP Tsai, and HR Sharma. Step-terrace morphology and reactivity to c60 of the five-fold icosahedral ag–in–yb quasicrystal. *Philosophical Magazine*, 91(19-21):2862–2869, 2011.

[21] Vincent Fournée, Émilie Gaudry, Julian Ledieu, Marie-Cécile De Weerd, Dongmei Wu, and Thomas Lograsso. Self-organized molecular films with long-range quasiperiodic order. *ACS nano*, 8(4):3646–3653, 2014.

[22] RC Haddon. The fullerenes: powerful carbon-based electron acceptors. *Philosophical Transactions of the Royal Society of London. Series A: Physical and Engineering Sciences*, 343(1667):53–62, 1993.

[23] Sam Coates, Joseph A Smerdon, Ronan McGrath, and Hem Raj Sharma. A molecular overlayer with the fibonacci square grid structure. *Nature Communications*, 9(1):3435, 2018.

[24] John Venables. *Introduction to surface and thin film processes*. Cambridge university press, 2000.

[25] George Frederick Weston. *Ultrahigh vacuum practice*. Elsevier, 2013.

[26] Austin Chambers. *Modern vacuum physics*. CRC Press, 2004.

[27] Zbigniew M Stadnik. *Physical properties of quasicrystals*, volume 126. Springer Science & Business Media, 1998.

[28] B Bolliger, M Erbudak, A Hensch, and DD Vvedensky. Surface structural phase transitions on icosahedral al–pd–mn. *Materials Science and Engineering: A*, 294:859–862, 2000.

[29] Gerd Binnig and Heinrich Rohrer. Scanning tunneling microscopy. *Surface science*, 126(1-3):236–244, 1983.

[30] Chunli Bai. *Scanning tunneling microscopy and its application*, volume 32. Springer Science & Business Media, 2000.

[31] Kenjiro Oura, VG Lifshits, AA Saranin, AV Zotov, and M Katayama. *Surface science: an introduction*. Springer Science & Business Media, 2013.

[32] C Julian Chen. *Introduction to Scanning Tunneling Microscopy Third Edition*, volume 69. Oxford University Press, USA, 2021.

[33] A Refik Kortan, Russell S Becker, FA Thiel, and HS Chen. Real-space atomic structure of a two-dimensional decagonal quasicrystal. *Physical review letters*, 64(2):200, 1990.

[34] Ignacio Horcas, Rs Fernández, JM Gomez-Rodriguez, JWSX Colchero, JWSXM Gómez-Herrero, and AM Baro. Wsxm: A software for scanning probe microscopy and a tool for nanotechnology. *Review of scientific instruments*, 78(1), 2007.

[35] Jan A. Czochralski. Ein neues verfahren zur messung der kristallisationsgeschwindigkeit der metalle. *Zeitschrift für Physikalische Chemie*, 92U:219 – 221, 1918.

[36] Birgitta Bauer, Götz Meisterernst, Juergen Haertwig, Thomas Schenk, and Peter Gille. Czochralski growth and x-ray topographic characterization of decagonal alconi quasicrystals. *Philosophical Magazine*, 86(3-5):317–322, 2006.

[37] Peter Gille, P Dreier, M Gräber, and T Scholpp. Large single-grain alconi quasicrystals grown by the czochralski method. *Journal of crystal growth*, 207(1-2):95–101, 1999.

[38] Jeremy Sloan, Rafal E Dunin-Borkowski, John L Hutchison, Karl S Coleman, V Clifford Williams, John B Claridge, Andrew PE York, Cigang Xu, Sam R Bailey, Gareth Brown, et al. The size distribution, imaging and obstructing properties of c60 and higher fullerenes formed within arc-grown single walled carbon nanotubes. *Chemical Physics Letters*, 316(3-4):191–198, 2000.

[39] Robert F Curl and Richard E Smalley. Probing c60. *Science*, 242(4881):1017–1022, 1988.

[40] Jean-Marie Dubois, Song Seng Kang, and Yvan Massiani. Application of quasicrystalline alloys to surface coating of soft metals. *Journal of non-crystalline solids*, 153:443–445, 1993.

[41] An-Pang Tsai, Akihisa Inoue, and Tsuyoshi Masumoto. New decagonal al–ni–fe and al–ni–co alloys prepared by liquid quenching. *Materials transactions, JIM*, 30(2):150–154, 1989.

[42] JY Park, DF Ogletree, M Salmeron, RA Ribeiro, PC Canfield, CJ Jenks, and PA Thiel. High frictional anisotropy of periodic and aperiodic directions on a quasicrystal surface. *Science*, 309(5739):1354–1356, 2005.

[43] Jean-Marie Dubois. Properties-and applications of quasicrystals and complex metallic alloys. *Chemical Society Reviews*, 41(20):6760–6777, 2012.

[44] Erik J Cox, Julian Ledieu, Ronan Mcgrath, Renee D Diehl, Cynthia J Jenks, and Ian Fisher. The ten-fold surface of the decagonal al 72 ni 11 co 17 quasicrystal studied by leed, spa-leed, aes and stm. *MRS Online Proceedings Library*, 643:1131–1136, 2000.

[45] S Burkardt, M Erbudak, and R Mäder. High-temperature surface oxidation of the decagonal alconi quasicrystal. *Surface science*, 603(6):867–872, 2009.

[46] HR Sharma, W Theis, P Gille, and KH Rieder. Faceting of the two-fold decagonal al71. 8ni14. 8co13. 4 (0 0 1 1 0) surface studied by he diffraction. *Surface science*, 511(1-3):387–391, 2002.

[47] HR Sharma, KJ Franke, W Theis, A Riemann, S Fölsch, KH Rieder, and P Gille. Investigation of the twofold decagonal al71. 8ni14. 8co13. 4 (1 0 0 0 0) surface by spa-leed and he diffraction. *Surface science*, 561(2-3):121–126, 2004.

[48] Wolfgang Theis, Eli Rotenberg, Katharina J Franke, Peter Gille, and Karsten Horn. Electronic valence bands in decagonal al-ni-co. *Physical Review B*, 68(10):104205, 2003.

[49] HR Sharma, KJ Franke, W Theis, P Gille, PH Ebert, and KH Rieder. Low-energy surface phonons of decagonal and icosahedral quasicrystals by inelastic he-atom scattering. *Physical Review B*, 68(5):054205, 2003.

[50] VA Rogalev, O Gröning, R Widmer, JH Dil, F Bisti, LL Lev, T Schmitt, and VN Strocov. Fermi states and anisotropy of brillouin zone scattering in the decagonal al–ni–co quasicrystal. *Nature Communications*, 6(1):8607, 2015.

[51] Harold W Kroto, James R Heath, Sean C O'Brien, Robert F Curl, and Richard E Smalley. C60: Buckminsterfullerene. *nature*, 318(6042):162–163, 1985.

[52] JA Smerdon, L Leung, JK Parle, CJ Jenks, R McGrath, V Fournée, and J Ledieu. Formation of a quasicrystalline pb monolayer on the 10-fold surface of the decagonal al–ni–co quasicrystal. *Surface science*, 602(14):2496–2501, 2008.

[53] W Allers, C Hahn, M Löhndorf, S Lukas, S Pan, UD Schwarz, and R Wiesendanger. Nanomechanical investigations and modifications of thin films based on scanning force methods. *Nanotechnology*, 7(4):346, 1996.

[54] S-L Chang, WB Chin, C-M Zhang, CJ Jenks, and PA Thiel. Oxygen adsorption on a single-grain, quasicrystal surface. *Surface science*, 337(1-2):135–146, 1995.

[55] JS Ko, AJ Gellman, TA Lograsso, CJ Jenks, and PA Thiel. Friction between single-grain al70pd21mn9 quasicrystal surfaces. *Surface Science*, 423(2-3):243–255, 1999.

[56] Vincent Fournée, Julian Ledieu, Émilie Gaudry, Hem-Raj Sharma, and Ronan McGrath. Ultra-thin films on complex metallic alloy surfaces: A perspective. *Recent Advances in Thin Films*, pages 13–34, 2020.

[57] J Ledieu, CA Muryn, G Thornton, RD Diehl, TA Lograsso, DW Delaney, and R McGrath. C60 adsorption on the quasicrystalline surface of al70pd21mn9. *Surface science*, 472(1-2):89–96, 2001.

List of Figures

1.1 A section of the one dimensional Fibonacci chain composed of long (L) and short (S) sections. In terms of this project, the circles represent atoms and the lines represent the spacing between them. 2

1.2 Model showing the periodic atomic spacing (2 Å) in the tenfold direction and the quasiperiodic atomic spacing (5 Å and 8 Å) in the twofold direction for the twofold surface of Al-Ni-Co. The blue represents aluminium and the grey represents the transmission metals nickel and cobalt. . . . 3

1.3 Model showing the separation of similar high density atomic planes in the twofold direction (5 Å and 8 Å). The blue represents aluminium and the grey represents the transmission metals nickel and cobalt. 4

1.4 This schematic diagram shows the way in which C_{60} is expected to adsorb onto the quasicrystaline surface, with this schematic using the surface of Al-Pd-Mn as an example. STM images are overlayed to show relation between substrate and overlayer. The yellow represents the twofold orientation and the pink represents the fivefold orientation. The red dots correspond to Mn atoms, to which C_{60} (green) preferentially adsorbs. Image from [23]. 6

2.1 Diagram shows the process of sputtering. Ar^+ ions are incident on the surface and removes the contamination, leaving a rough surface. 8

2.2 Diagram shows the process of annealing. The surface is heated and becomes flat. Through providing energy to the bulk the surface reaches a state closer to equilibrium. 9

2.3 A schematic of the path the STM tip takes as it measures d, the distance between the tip and the surface. This diagram shows observation of ultra fine metal particles in the constant current mode. Image from [30]. . . 9

3.1 A: STM image of the clean surface with multiple clear terraces. An area that contains a change in terrace is highlighted. The highlighted area has been plane flattened to achieve the most accurate step height data. Figure B represents a histogram of the Z heights for figure A. It plots the frequency for each Z height, thus the peaks give the most common Z heights for the image. The step height is therefore measured as the difference in Z between the histogram peaks. 14

3.2 Histogram showing the frequency of given step heights for the clean surface. There are clear peaks at 5 Å and 8 Å. 15

3.3 STM images of the clean surface covering areas of the same size. A shows the surface before dosing, B shows the clean surface after dosing. Both images have been plane flattened. The surface before dosing does not show atomic resolution unlike the surface after dosing. There are fewer rows visible in the surface prior to dosing, with only those especially bright discernible. 16

3.4 A: an STM image of the clean part of the surface after dosing which has a ruler with the short and long atomic spacings overlayed. B: The clean surface before dosing, with a ruler overlayed showing the spacing present on the surface. Here the average long and short values were used (as described in section 3.1.3), with $S = 0.525$ nm and $L = 0.768$ nm. The dashed lines connects the segments between the two surfaces. . . . 17

3.5 A: the frequency of atomic distances along the periodic direction for the surface before dosing. B the frequency for the substrate after dosing. There are clear peaks at the expected 2 Å and multiples of 2 Å. 18

3.6 The frequency of aperiodic atomic distances for the clean surface before dosing (A) and after dosing (B). 19

3.7 The dosed surface with instances of the two C_{60} molecule (thumbprint) motif highlighted with an enlarged example of one such 'thumb print'. . 20

3.8 An example of a light C_{60} adsorption site is highlighted. The substrate surrounding the site is shown to be lighter in colour. 21

3.9 An example of a dark C_{60} adsorption site is highlighted. The substrate surrounding the C_{60} is notably darker than in figure 3.8. 21

3.10 Three to four C_{60} molecules adsorbed in a chain in the periodic directions are highlighted, with one example enlarged. 22

3.11 Possible adsorption sites for the chain motif (as seen in figure 3.10) on the model with an STM example of the motif alongside. The model shows the periodic and quasiperiodic directions aligning with the vertical and horizontal directions respectively. In the model, the green represents the C_{60}, the blue represents aluminium atoms and grey represents nickel and cobalt atoms. The long and short spacings are labelled, with the C_{60} shown to adsorb in the LL sites. 23

A.1 On the left, a low magnification STM image of the surface of the twofold plane. This shows large terraces and straight steps are observed along the tenfold direction. Points A and B are presented for the height profile, as shown on the right. Figures from reference [5]. xiii

A.2 (a) STM images (14.5nm x 9nm) of two contiguous regions in the twofold Al-Ni-Co surfaces, this image shows the complete Fibonacci sequence. Here it is shown that the terraces are composed of rows of periodically arranged atoms (0.4nm) along the tenfold direction, separated by distances L and S. (b) shows the interior in the L and S sections. (c) is the sequence of L and S spacings between rows, showing that it follows a Fibonacci sequence. Images from [6]. xiv

A.3 Structure of C_{60}, the molecule has a diamater of 0.7 nm [38]. Image from [39]. xvii

A.4 LEED patterns of the clean tenfold Al-Ni-Co surface decagonal phase before the addition of C60 (a) and the LEED patterns of the C60 molecular film formed on that surface (b). Image from reference [21]. xviii

A.5 Quasicrystalline C_{60} on the two-fold Al-Pd-Mn quasicrystal, imaged by STM. A Fibonacci square grid of S = 1.26nm, L = 2.04nm, to highlight the ordering of C_{60}. Figure taken from [23]. xix

B.1 The image on the left shows a plane flattened STM images containing multiple terraces which are labelled A through D. The corresponding histogram is shown in the right, with the same terraces labelled. xx

B.2 The image on the left shows a flattened STM image displaying the rows of atoms on the surface. The line profile tool has been used across the line seen on the image to produce the graph shown on the right. The graph shows the given height of the surface at a particular distance along the line. xxii

B.3 STM image with a line drawn across. This was the line across which the line profile was drawn (figure B.4). Each atomic row in the horizontal direction has been labelled alphabetically. xxiii
B.4 Line profile of figure B.3. It shows the height of the surface at a given distance along the line. This was used to measure the distance between points of interest. xxiv
B.5 Section of the undosed clean surface that was related to the dosed clean surface. The line profile is shown on the right, the atomic rows (which correspond to peaks on the line profile) are numbered alphabetically . . xxiv
B.6 Clean surface before dosing with a ruler overlayed to show to distances between clear atomic sites in terms of L and S. xxiv
B.7 The left shows a thumbprint of C_{60} with the region above it selected. This region is shown on the right. The image has been flattened, the atomic rows labelled alphabetically and a line profile was taken from the line shown. This line profile is shown in figure B.8. xxviii
B.8 Line profile of figure B.7. It shows the height of the surface at a given distance along the line. This was used to measure the distance between atomic rows. xxix
B.9 Thumbprint on a light adsorption site (left) with a line profile drawn from the line (right). xxx
B.10 Thumbprint on a dark adsorption site (left) with a line profile drawn from the line (right). xxx

List of Tables

1.1 The periodic, long and short atomic distances as calculated from the model (figure 1.2). 3
1.2 The expected step heights between terraces from the model (figure 1.3). 4

3.1 The average step height measured for the short (S) and long (L) steps. The errors were determined from the spread of the values measured. . . 15
3.2 The average periodic atomic distances for the surface before and after dosing. The errors were determined from the spread of the values measured. 18
3.3 The average aperiodic atomic distances (S and L) for the clean surface before and after dosing. The errors were determined from the spread of the values measured. 19

A.1 Table of studies of qasicrystalline Al-Ni-Co and the annealing temperatures used. xvi

B.1 Change in step height between terraces as read from the histogram in figure B.1. xxi
B.2 Results of the spacing between different atomic rows labelled A-G as shown in figure B.3. The series of short and long sections between two points is listed along with the S + L combination requried to go between the two points. xxv
B.3 Average spacing for different L + S combinations. An error of 0.25 nm can be assumed for all values. xxvi
B.4 Distances between the points in figure B.5. xxvii
B.5 Distance between the atomic rows from figure B.8. xxix

Appendices

Appendix A

Literature Review

A.1 Quasicrystals and Al-Ni-Co

Quasicrystals are structures which do not exhibit periodicity but do possess long range order. They were first observed in 1984 by Shechtman et al. [1], where it was seen that they had long-range crystallographic order, as observed by the tenfold Bragg peaks of the icosahedral point group symmetry, inconsistent with conventionally accepted lattice translations. This interesting symmetry showed that while the surface exhibited symmetries associated with conventional crystals (e.g. twofold), it also exhibited forbidden symmetries (e.g. fivefold). In addition to unconventional symmetry, quasicrystals process interesting physical properties, such as corrosion, oxidation, and wear resistance, as demonstrated by Dubois et al. [40].

This project focuses on the twofold symmetry observed in Al-Ni-Co. In 1989, Tsai et al. [41] discovered that a two dimensional quasicrystal with decagonal structure was found to form in Al-Ni-Co alloys. The structure was found to have both twofold and tenfold symmetry. In 2002, STM was first reported for this structure by Kishida et al. [5], where STM was used to image the twofold plane as presented in figure A.1. The authors observed straight steps which are oriented exactly to the tenfold direction. The height profile is presented in figure A.1, which shows that there are two different step heights, termed L and S. The ratio between L and S is approximately τ (where $\tau = \frac{1+\sqrt{5}}{2}$), meaning the sequence agrees with the Fibonacci sequence. It was also observed that the sequence of the different step heights is aperiodic, consistent with the fact the decagonal quasicrystal has quasiperiodic order in the twofold direction.

Park et al. [6] further investigated the atomic structure of the twofold surface of decagonal Al-Ni-Co using STM. This paper corrobortated that the surface has terraces

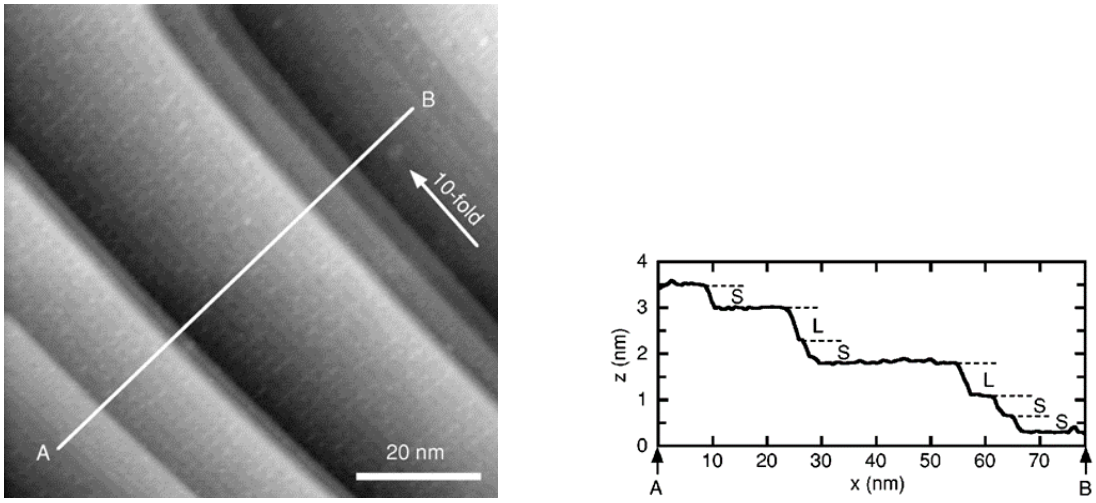

Figure A.1: On the left, a low magnification STM image of the surface of the twofold plane. This shows large terraces and straight steps are observed along the tenfold direction. Points A and B are presented for the height profile, as shown on the right. Figures from reference [5].

(flat regions on the surfaces) which are separated by steps (small changing in height), containing rows of atoms parallel to the tenfold direction. These rows were observed to be arranged aperiodically with separations that follow a Fibonacci sequence and inflation symmetry. This arrangement is such that the surface has periodicity in the direction along the tenfold axis but is aperiodic in the perpendicular direction, which was imaged by Park et al. as shown in figure A.2. This surface has proved to have interesting properties, with the friction along the aperiodic direction being considerably less than along the periodic, again demonstrated by Park et al. [42]. Properties such as this have shown to provide providing interesting applications for quasicrystals, such as extending the lifetime of certain tools, as explored by Dubois [43].

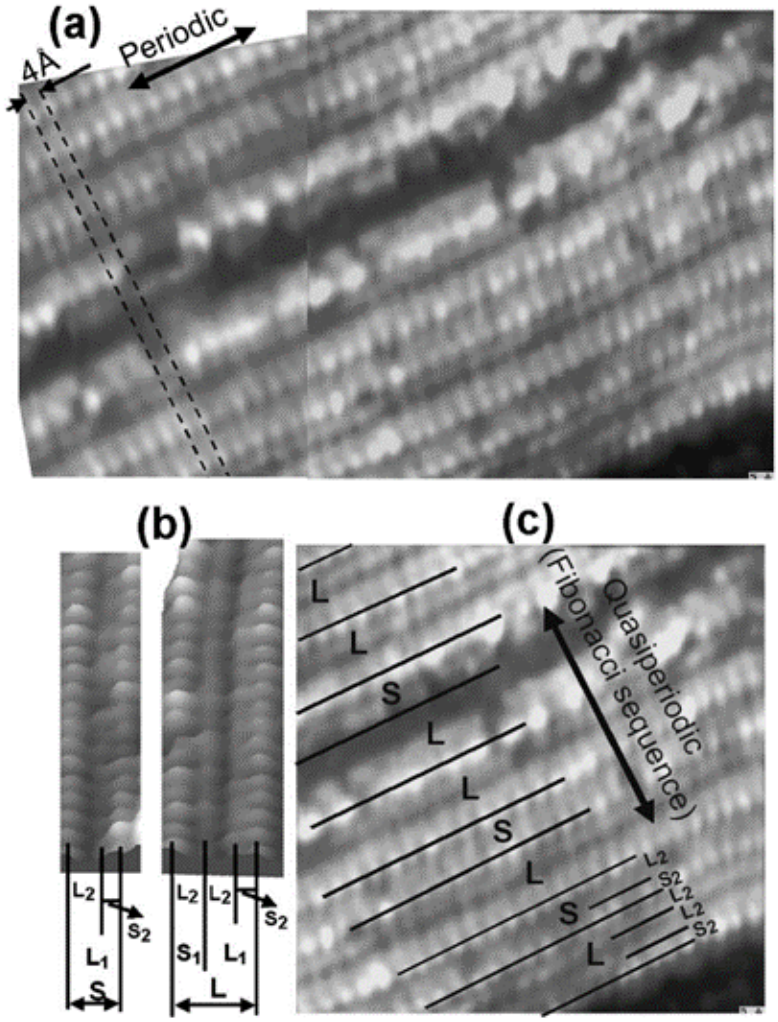

Figure A.2: (a) STM images (14.5nm x 9nm) of two contiguous regions in the twofold Al-Ni-Co surfaces, this image shows the complete Fibonacci sequence. Here it is shown that the terraces are composed of rows of periodically arranged atoms (0.4nm) along the tenfold direction, separated by distances L and S. (b) shows the interior in the L and S sections. (c) is the sequence of L and S spacings between rows, showing that it follows a Fibonacci sequence. Images from [6].

A.2 Techniques and Requirements

In order for this project to be carried out successfully it is essential that the correct conditions for preparation and analysis are met, and the appropriate techniques are used. The sample will be prepared and analysed under Ultra-High Vacuum (UHV)

conditions, generally defined as pressures below 10^{-8} mbar. This is to avoid any contamination of the surface from ambient gasses (for example oxidation), allowing the surface to be kept clean over the period of the experiment [25]. It is also important in reducing the number of particles which could interact with the probe and disturb the measurement. Using UHV increases the mean free path of any electrons in the chamber as there are virtually no particles with which to collide, meaning that any interactions will be with the surface inside the UHV chamber. The preparation of the surface as well as the STM analysis must take place in UHV [24], so it is essential that our chamber is prepared carefully. UHV conditions are created and maintained using multiple pumps to remove any particles within the chamber [26]. All studies discussed within this review conducted their preparation and analysis under UHV conditions.

The main technique used in analysis for this project will be Scanning Tunnelling Microscopy (STM). This is a technique which was discovered by Binnig and Rohrer [29] in 1982. It is used to observe the surfaces of materials, allowing for the imaging of individual atoms or molecules [30]. STM achieves a high spatial resolution using the quantum phenomenon of electron tunnelling. It uses an extremely sharp tip which is brought close to the surface and a bias volage applied, the potential difference between the tip and the surface allows electrons to tunnel between them. A tunnelling current arises, which depends exponentially on the distance between the tip and the surface. Through measuring this the topography of the sample can be mapped, allowing for the surface to be imaged [32]. STM has been used widely in the study of quasicrystals, with the first example for Al-Ni-Co, done by Kishida et al. [5], as described earlier.

For this project, surface preparation is essential to understand the clean surface properties. The surface needs to be cleaned as, when exposed to air, an oxide layer a few nm thick forms, as described by Thiel et al. [27]. This layer of surface impurities (which includes other air-born contaminants as well as oxygen) needs to be removed, which is done through a process of sputtering and annealing: a process whereby the surface is bombarded with ions and heated in order to remove any impurities from the surface. The process of annealing also provides energy to the bulk of the sample, allowing it to rearrange into a state closer to equilibrium, changing the structure of the surface. This is a process that is repeated for many cycles under UHV. The temperature for annealing is critical, as too low will yield a poor-quality surface (due to improper removal of impurities, or due to not enough energy supplied for rearrangement of the bulk), but too high can cause phase changes or melting, which could permanently alter the struture, as described by Sharma et al. [14]. When the optimal temperature is used, a surface with a near bulk composition and a step terraced surface can be

obtained. Sharma et al. [14] proposed after a review of the structure and growth of these surfaces that an optimal temperature for annealing for Al-Ni-Co is 700-900 °C. The impacts of different annealing temperatures have been explored by Cox et al. [44] who annealed at 400-900 °C. It was found that the temperature must be greater than 450 °C for the observation of terraces, and the terraces increased in size at higher annealing temperature, with 600°C showing improved quality of STM and LEED (Low Energy Electron Diffraction) images. The upper limit of annealing was described by Park et al. [6], who found that the surface undergoes a phase transformation above 925 °C. For this project, an initial annealing temperature of 650 °C was chosen, above the threshold for improved terraces as found by Cox et al. [44], but below the phase transition found by Part et al. [6]. Starting at this temperaure ensures that there is reduced risk of melting and this temperature will be reassessed after the first round of imaging. This decision was also supported by the studies shown in table A.1, which annealed at similar temperatures.

Author (year)	Composition	Temperature (°C)
Cox et al. (2005) [44]	$Al_{72}Ni_{11}Co_{17}$	400-900
Burkardt et al. (2008) [45]	$Al_{72.9}Ni_{10.4}Co_{16.7}$	600
Sharma et al. (2002) [46]	$Al_{71.8}Ni_{14.8}Co_{13.4}$	600-650
Sharma et al. (2004) [47]	$Al_{71.8}Ni_{14.8}Co_{13.4}$	600-650
Theis et al. (2003) [48]	$Al_{71.8}Ni_{14.8}Co_{13.4}$	600-800
Fournée et al. (2014) [21]	$Al_{72.1}Ni_{10.6}Co_{17.3}$	625-750
Sharma et al. (2003) [49]	$Al_{71.8}Ni_{14.6}Co_{13.4}$	650
Rogalev et al. (2015) [50]	$Al_{70}Ni_{20}Co_{10}$	750

Table A.1: Table of studies of qasicrystalline Al-Ni-Co and the annealing temperatures used.

A.3 Deposition of C_{60}

C_{60} (also known as buckminsterfullerene) was first discovered in 1985 by Kroto et al. [51]. The molecule has a spherical-like structure containing sixty carbon atoms, with the shape being made up of 12 pentagons and 20 hexagons, with a carbon atom at the vertices of each polygon (and a bond along each polygon edge), as shown in figure A.3. C_{60} molecules are desirable for STM imaging as they are large and isotropic, making them easier to image.

C_{60} is regularly used in the context of quasicrystals, such as a probing element (as used by Smerdon et al. [52]) and also directly deposited onto the quasicrystalline surfaces. It is widely chosen to deposit onto the surface of quasicrystals as it is a

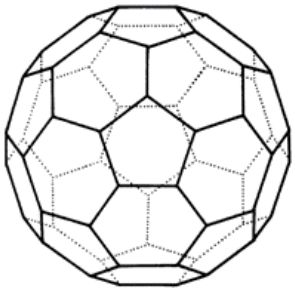

Figure A.3: Structure of C_{60}, the molecule has a diamater of 0.7 nm [38]. Image from [39].

good electron acceptor, as described by Haddon et al. [22], meaning a strong electronic molecule-substrate interaction is expected. C_{60} is further favourable for deposition as it improves the frictional propertoes of the surface, which was described by Allers et al. [53]. Unlike common adsorbates such as oxygen and sulphur, C_{60} does not cause immediate disordering of the surface [54, 55] which could lead to displacement adsorption, affecting the surface structure. Quasicrystals have been consistently used as a substrates for thin film growth, as described in a review by Fournée et al. [56]. The first studies involving C_{60} used the molecules as a marker, indicating the preferred tenfold surface. This is demonstrated by Ledieu et al. [57], where C_{60} was adsorbed at room temperature onto the quasicrystal surface Al-Pd-Mn.

As this project involves the first deposition of C_{60} onto the twofold quasicrystalline surface of Al-Ni-Co, the studies used in this literature review will focus on either the tenfold surface of the same alloy, or on similar quasicrystals with different elemental compositions.

A study of particular note is one performed by Fournée et al. [21] in 2014, where the authors grew molecular films of C_{60} onto aluminium based quasicrystals, including the tenfold Al-Ni-Co surface. It was observed that the LEED image taken of the molecular film had similar characteristics to the LEED taken before the deposition of C_{60}, as shown in figure A.4. This suggested to the authors that the C_{60} monolayer had self-organised into a tenfold symmetric pattern. A similar result was observed for the tenfold surface of Al-Cu-Co. It was found that the pentagonal tiles formed by the molecular film matched the dimensions of the underlying quasiperiodic tiling. This suggested that the C_{60} molecules were preferentially adsorbing at the fivefold symmetric sites. The author's performed DFT (density functional theory) calculations and found that the most favourable adsorption configurations at these sites corresponded to the molecules contacting the substrate with the electron deficient carbon face, allowing for efficient

electron transfer from substrate to C_{60}. The author's concluded that these behaviours are likely to specific to quasicrystals and their approximants.

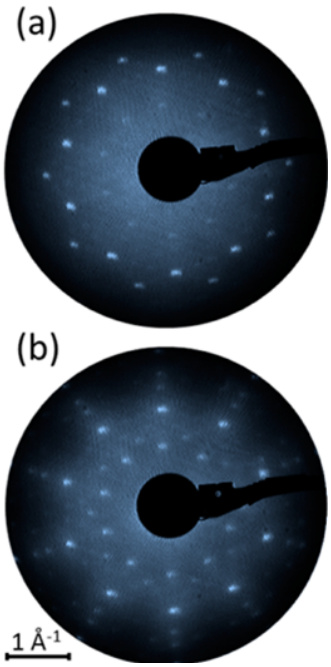

Figure A.4: LEED patterns of the clean tenfold Al-Ni-Co surface decagonal phase before the addition of C60 (a) and the LEED patterns of the C60 molecular film formed on that surface (b). Image from reference [21].

This project endeavours to achieve site specific adsorption using C_{60} and observe this using STM. This has been demonstrated for Al-Pd-Mn by Coates et al. [23]. The authors observed a Fibonacci square grid structure of Al-Pd-Mn through the adsorption of C_{60} on to the Mn atoms. This was achieved and was observed using STM. The STM image of the grid is shown in figure A.5. The site-specific adsorption was due to C_{60} being a good electron absorber and Mn being electron rich, allowing for the preferential adsorption displayed. Through this study it was shown that C_{60} can be used as a chemical probe, adsorbing to specific sites of a complex structure and providing insight into the surface structure. This project will pursue a similar goal, aiming to observe site absorption of C_{60} molecules on Al-Ni-Co, with the hypothesis that there will be preferential adsorption of C_{60} onto nickel, as it has similar electronic configuration to Manganese, and so is expected to behave similarly. This project aims to produce the first demonstrated atomic chain of aperiodically arranged atoms by deposition, which are expected to follow a Fibonacci sequence.

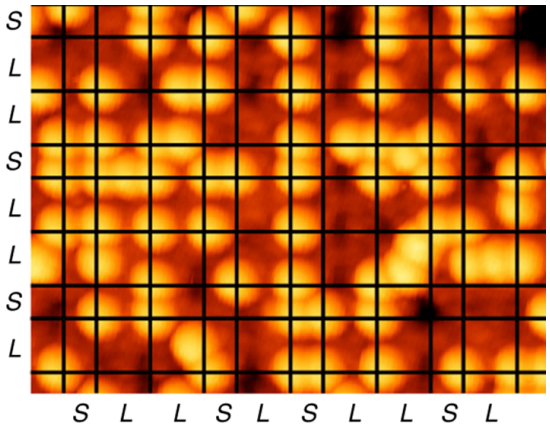

Figure A.5: Quasicrystalline C_{60} on the two-fold Al-Pd-Mn quasicrystal, imaged by STM. A Fibonacci square grid of S = 1.26nm, L = 2.04nm, to highlight the ordering of C_{60}. Figure taken from [23].

Appendix B

Analysis

B.1 Step Height Example

An example involving the "half step", as noted in the method, is shown, along with the corresponding histogram, in figure B.1. The terrace labelled C is relatively small, as shown by the small peak in the histogram. The step height is also shown to be below expectations when analysed (table B.1). When C is ignored, the step height aligns with expectations.

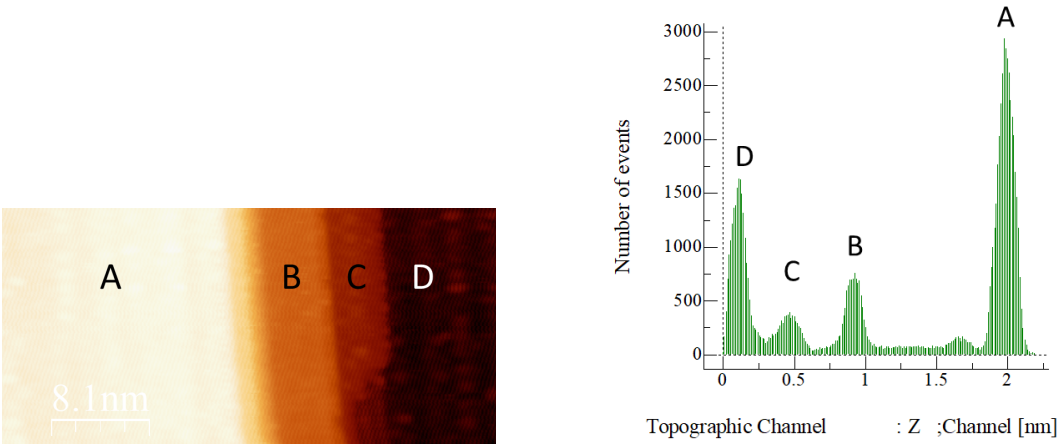

Figure B.1: The image on the left shows a plane flattened STM images containing multiple terraces which are labelled A through D. The corresponding histogram is shown in the right, with the same terraces labelled.

Step	Change in Z (nm)
A to B	1.048
B to C	0.469
C to D	0.356
B to D	0.822

Table B.1: Change in step height between terraces as read from the histogram in figure B.1.

B.2 Surface Ordering Example

To characterise the surface ordering a section with clear rows was selected and flattened as shown in figure B.2. In WSxM the line profile tool was used to plot the height vs the position to analyse the distances between the topographical peaks. The distances between the peaks (which should lie in the centre of the rows) were recorded for both the periodic and aperiodic direction. The frequencies of the atomic distances for each direction were recorded and plotted in order to determine the most common spacings.

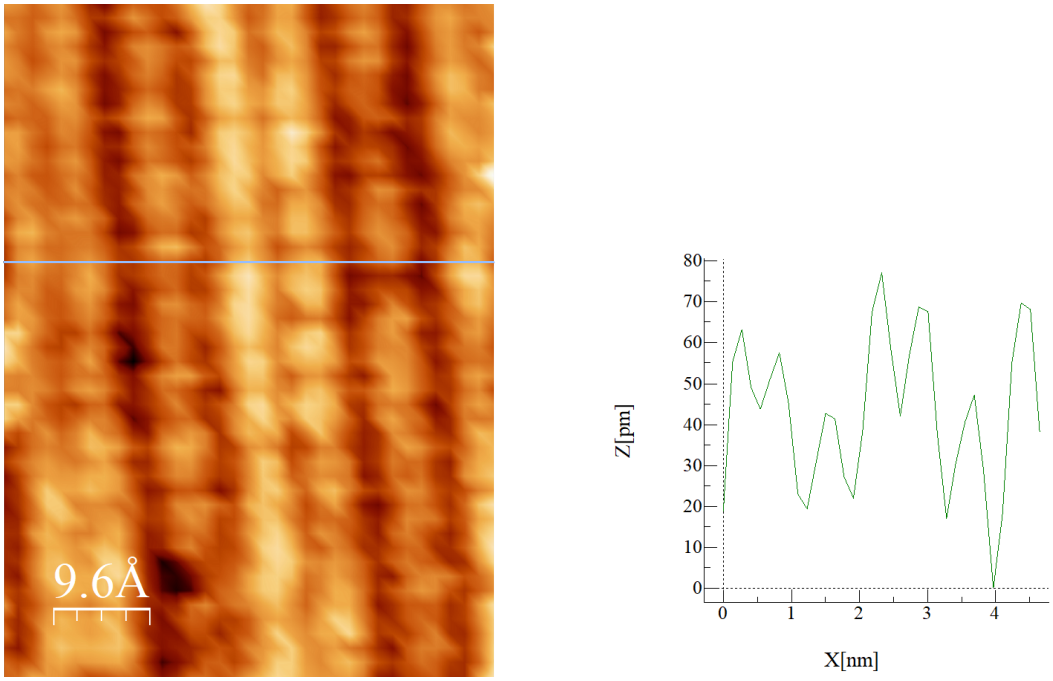

Figure B.2: The image on the left shows a flattened STM image displaying the rows of atoms on the surface. The line profile tool has been used across the line seen on the image to produce the graph shown on the right. The graph shows the given height of the surface at a particular distance along the line.

B.3 Relating Clean and Dosed Surfaces Example

Using the clean section of the dosed surface (figure B.3), the atomic distances were measured with the line profile tool (as shown in figure B.4).

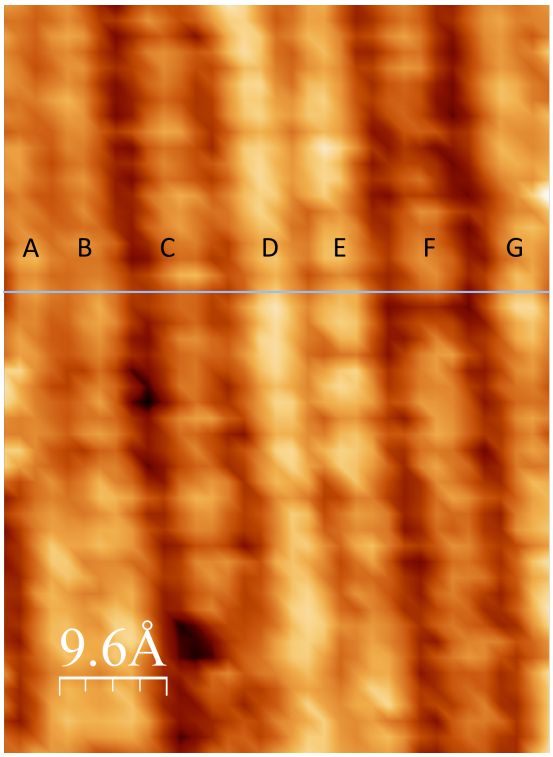

Figure B.3: STM image with a line drawn across. This was the line across which the line profile was drawn (figure B.4). Each atomic row in the horizontal direction has been labelled alphabetically.

For this image the distances were recorded, along with the kind of gap observed, as shown in table B.2. This was repeated for many images and an average for different combinations of S + L was taken. The averages are found in table B.3.

This was done similarly for the undosed surface as shown in figure B.5, and then the distances measured were compared. For this example the distances between points are listed in table B.4. The final result for this image is shown in figure B.6.

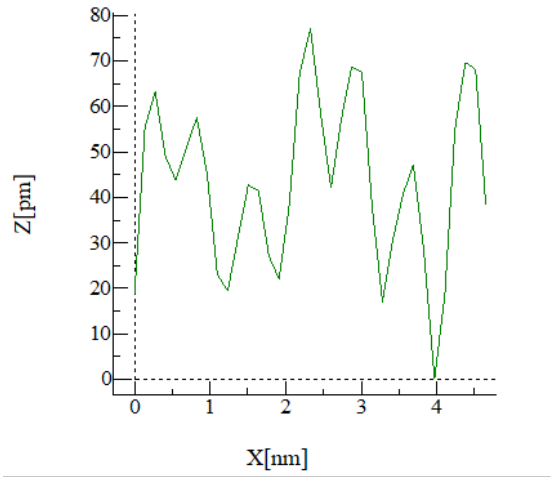

Figure B.4: Line profile of figure B.3. It shows the height of the surface at a given distance along the line. This was used to measure the distance between points of interest.

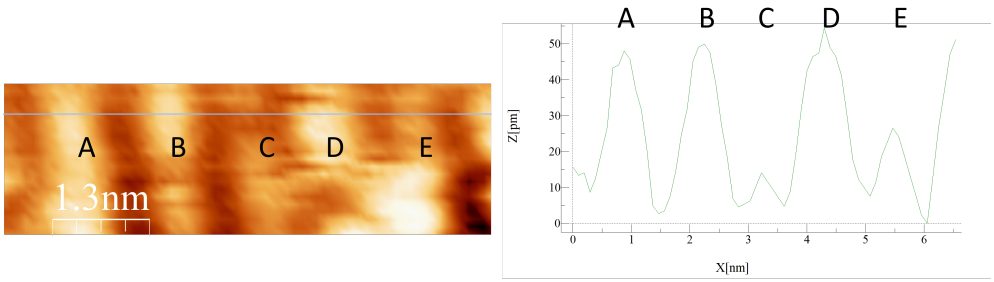

Figure B.5: Section of the undosed clean surface that was related to the dosed clean surface. The line profile is shown on the right, the atomic rows (which correspond to peaks on the line profile) are numbered alphabetically

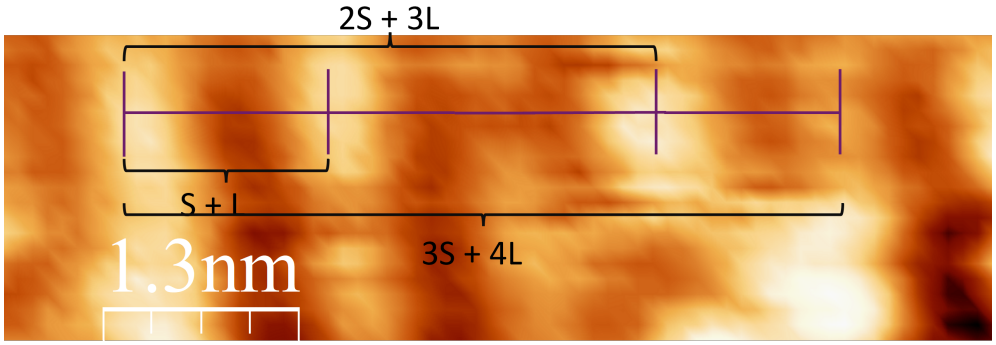

Figure B.6: Clean surface before dosing with a ruler overlayed to show to distances between clear atomic sites in terms of L and S.

Points	Distance Between Points (nm)	Type of Gap	S + L
A to B	0.495	S	1S 0L Y
A to C	1.272	SL	1S 1L Y
A to D	2.043	SLL	1S 2L Y
A to E	2.622	SLLS	2S 2L Y
A to F	3.338	SLLSL	2S 3L Y
A to G	4.12	SLLSLL	2S 4L Y
B to C	0.735	L	0S 1L Y
B to D	1.495	LL	0S 2L Y
B to E	2.063	LLS	1S 2L Y
B to F	2.848	LLSL	1S 3L Y
B to G	2.583	LLSLL	1S 4L Y
C to D	0.766	L	0S 1L Y
C to E	1.328	LS	1S 1L Y
C to F	2.102	LSL	1S 2L Y
C to G	2.843	LSLL	1S 3L Y
D to E	0.526	S	1S 0L Y
D to F	1.303	SL	1S 1L Y
D to G	2.085	SLL	1S 2L Y
E to F	0.786	L	0S 1L Y
E to G	1.534	LL	0S 2L Y
F to G	0.777	L	0S 1L Y

Table B.2: Results of the spacing between different atomic rows labelled A-G as shown in figure B.3. The series of short and long sections between two points is listed along with the S + L combination requried to go between the two points.

S + L	Average Spacing (nm)
1S 0L	0.525
0S 1L	0.767
1S 1L	1.308
0S 2L	1.525
2S 1L	1.817
1S 2L	2.086
2S 2L	2.609
1S 3L	2.830
2S 3L	3.360
1S 4L	3.352
3S 3L	3.917
2S 4L	4.153
2S 5L	5.003
3S 4L	4.758
3S 5L	5.540
4S 5L	6.113
3S 6L	6.340
4S 6L	6.872
3S 7L	7.103
5S 6L	7.404
4S 7L	7.629
5S 7L	8.180
4S 8L	8.184
4S 9L	8.732
5S 8L	8.940
6S 8L	9.527
5S 9L	9.695
5S 10L	10.427
6S 9L	10.294
7S 9L	10.923
6S 10L	11.031
7S 10L	11.707
6S 11L	11.776
6S 12L	12.528
8S 11L	13.103

Table B.3: Average spacing for different L + S combinations. An error of 0.25 nm can be assumed for all values.

Points	Distance between points (nm)
A to B	1.316
A to C	2.362
A to D	3.428
A To E	4.679
B to C	0.977
B to D	2.078
B to E	3.299
C to D	1.066
C to E	2.267
D to E	1.271

Table B.4: Distances between the points in figure B.5.

B.4 Determining C_{60} Position Example

Using the "thumbprint" depositions of C_{60}, the clean area surrounding the molecules was used to determine if there was any preferential adsorption. An example is shown in fugure B.7. Here the area above the thumbprint has been isolated to determine where

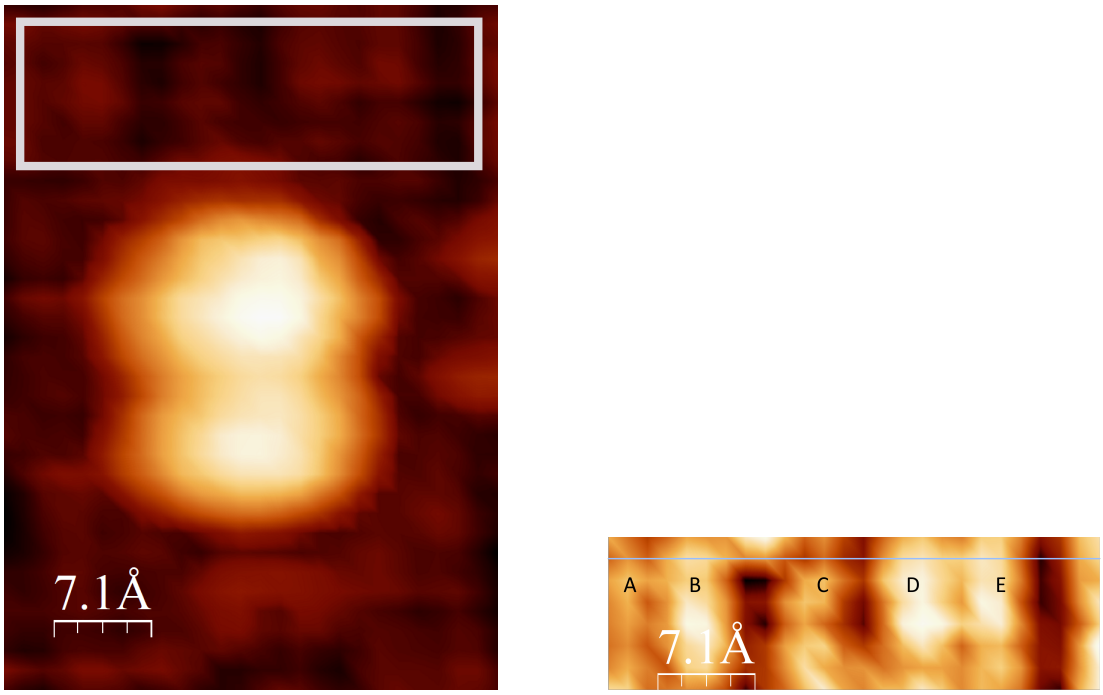

Figure B.7: The left shows a thumbprint of C_{60} with the region above it selected. This region is shown on the right. The image has been flattened, the atomic rows labelled alphabetically and a line profile was taken from the line shown. This line profile is shown in figure B.8.

the C_{60} has deposited. This is explored using a line profile, as shown in figure B.8.

The distances as measured using figure B.8 are shown in table B.5. From this it is clear that the middle spacing, corresponding to where the C_{60} has deposited (around C and D in figure B.7) is at the LL position.

To compare the height between light and dark sites a line profile was used. The light is shown in figure B.9 and dark is shown in figure B.10. There is a 1 Å difference in maximum between light and dark, with light being higher.

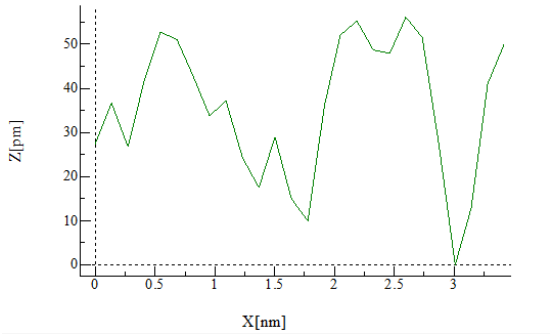

Figure B.8: Line profile of figure B.7. It shows the height of the surface at a given distance along the line. This was used to measure the distance between atomic rows.

Gap	Distance (nm)
A TO B	0.476
A TO C	1.34
A TO D	2.062
A TO E	2.59
B TO C	0.831
B TO D	1.541
B TO E	2.072
C TO D	0.742
C TO E	1.276
D TO E	0.534

Table B.5: Distance between the atomic rows from figure B.8.

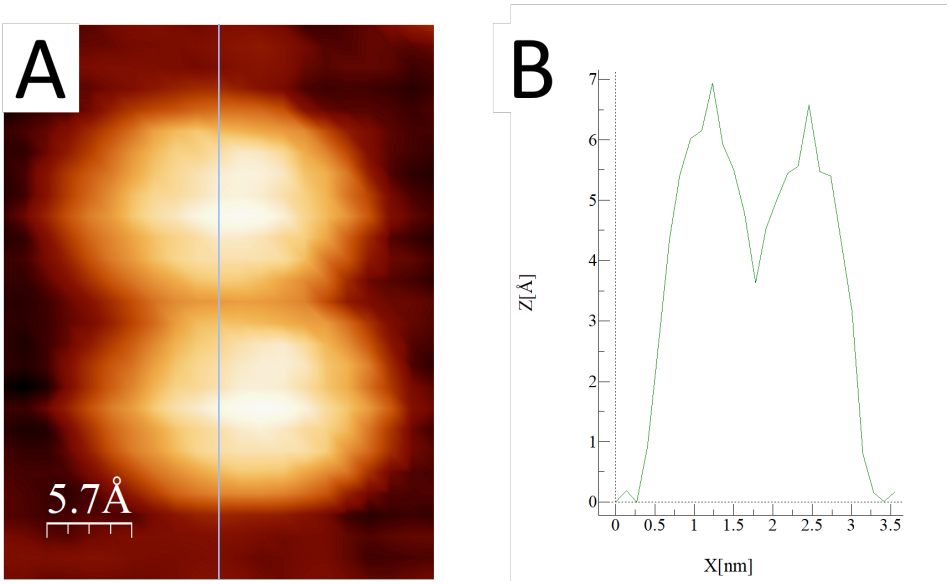

Figure B.9: Thumbprint on a light adsorption site (left) with a line profile drawn from the line (right).

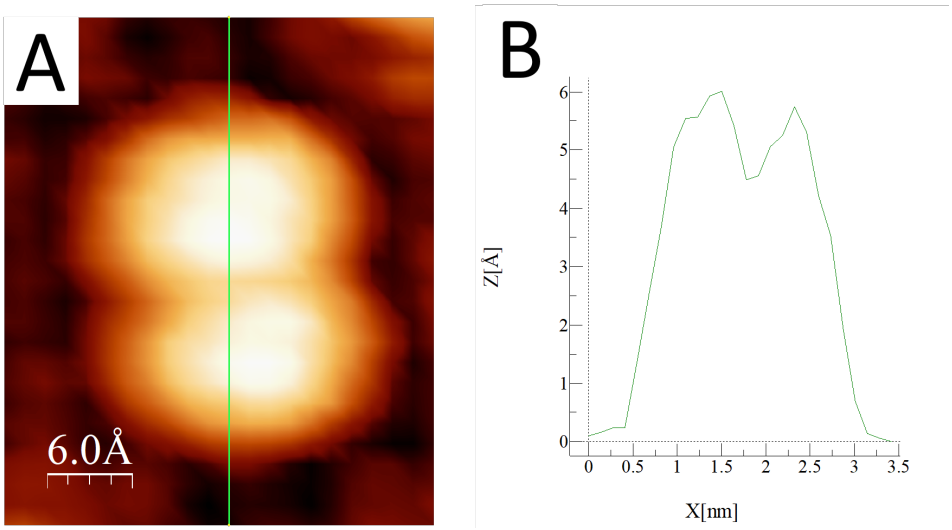

Figure B.10: Thumbprint on a dark adsorption site (left) with a line profile drawn from the line (right).